[^{11}C]Me-DPA for TSPO imaging, synthesis of boronic ester precursor for labeling with [^{11}C]CH_3

Master's Thesis
University of Turku
MSc Degree Program in Biomedical Sciences
Medicinal and Radiopharmaceutical Chemistry
(July 2020)

Adeleh Zaferanloo
Dr. Thomas Keller
Professor Olof Solin
PET Centre, Department of Chemistry

Abstract

UNIVERSITY OF TURKU
Faculty of Science and Engineering
Department of Chemistry and Turku PET Centre

ZAFERANLOO, ADELEH: [^{11}C]Me-DPA for TSPO imaging, Synthesis of boronic ester for labeling with [^{11}C]CH_3
Master´s Thesis, 39 p, 2 Appendices
MSc Degree Program in Biomedical Sciences, Medicinal and radiopharmaceutical Chemistry
July 2020

The translocator protein 18 kDa (TSPO) is overexpressed during neuroinflammation. TSPO- targeting tracers can be used to study neuroinflammation in diseases such as Alzheimer's disease (AD) and stroke. [^{18}F]F-DPA, a TSPO-specific tracer, is a recently developed analogue of [^{18}F]DPA-714 and it was developed to improve the metabolic stability. The methylated version has been previously reported to have a high binding affinity. Hence, in this study the necessary precursor is synthesized and labeled with [^{11}C]iodomethane.

The purpose of this study is to synthesize a suitable precursor for labeling with [^{11}C]CH_3I and to introduce the [^{11}C]CH_3 group onto the same position that is fluorinated [^{18}F]F-DPA.

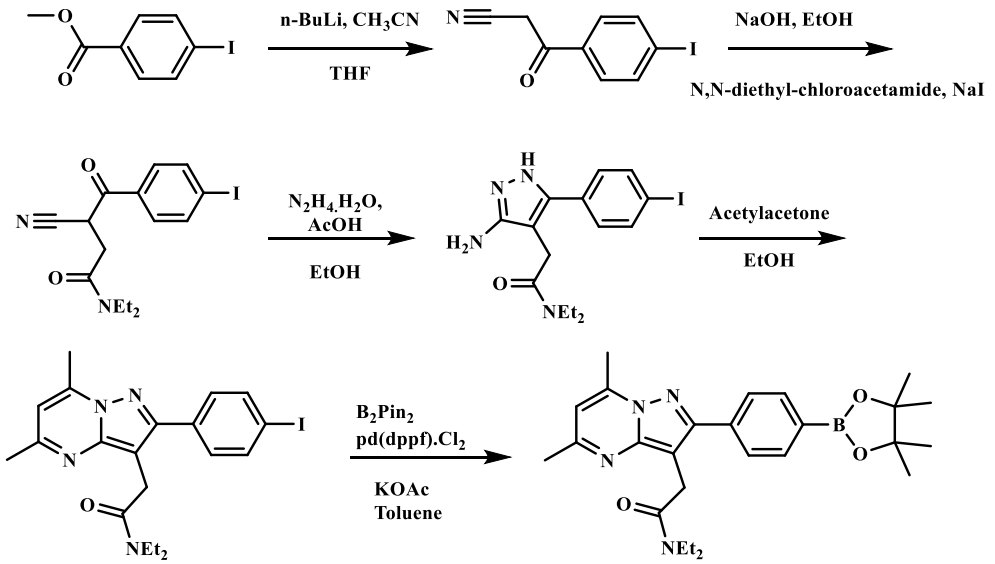

The advantage of labeling with carbon-11 is to avoid using electrophilic and nucleophilic ^{18}F-fluorination which have limitations during syntheses. Due to the F-DPA fast wash out, it would be suitable to label it with carbon-11.
The pinacol boronic ester precursor was made successfully; although, 3-cyano-*N*,*N*-diethyl-4- (iodophenyl)-4-oxobutanamide and pinacol boronic ester productions were time consuming and challenging especially the purification process.
Keywords: [^{18}F]F-DPA, TSPO, [^{11}C]Me-DPA, [^{11}C]CH_3I

Table of Contents

1. Introduction

A radioactive tracer is a compound in which one atom has been replaced with a radioisotope. Tracking the radioactivity generated by this compound during decay enables the study of physiological and pharmacological mechanisms and operations in the human body.[1]

Radioisotopes of hydrogen (H), carbon (C), nitrogen (N), oxygen (O), fluorine (F), phosphorus (P), sulfur (S), technetium (Tc), iodine (I), etc. can be used to track the distribution of a substance in biological systems such as cells and tissues by Positron Emission Tomography (PET), Single-Photon Emission Computed Tomography (SPECT, or SPET), and technetium scans. [1][2]

The translocator protein (TSPO) with a molecular weight of 18 kDa [3], is an outer mitochondrial membrane protein [4]. TSPO-specific ligands are commonly used for brain imaging and this is due to the high expression of TSPO during neuroinflammation. TSPO is involved in cholesterol and porphyrin transport and plays a significant role in apoptosis [5][6].

DPA-714 is a ligand of TSPO which has a high affinity of (K_i=7 nM) [7]. [^{18}F]DPA-714 labeled with fluorine-18 has been used in PET imaging of brain tumors and neuroinflammation [8]. However is has been shown that this radiotracer is metabolically unstable and a more metabolically stable analogue, [^{18}F]F-DPA, was developed [9].

In F-DPA the fluorine atom is connected to the structure directly without a linker. The metabolism of [^{18}F]DPA-714 lead to the cleavage of the radioactive label and the formation of non-specifically binding radioactive metabolites [10]. [^{18}F]F-DPA was first synthesized by electrophilic fluorination [9] and nucleophilic syntheses have been developed by many research groups [11][12][13]. The evaluation in rats showed that the tracer had good entry into the brain and a fast washout, so that equilibrium was reached 20-40 min after tracer injection [9]. Furthermore, comparison between brain samples of animals injected with [^{18}F]F-DPA or [^{18}F]DPA-714 showed that [^{18}F]F-DPA had a higher metabolic stability compared to [^{18}F]DPA-714. Moreover, it has also been used successfully to study neuroinflammation in a mouse model of AD [10].

The aim of this research is to synthesize a suitable precursor for labeling with [^{11}C]CH_3I and to introduce the [^{11}C]CH_3 group onto the same position that is fluorinated in [^{18}F]F-DPA.

2. Literature review

2.1. Nuclear Medicine

Nuclear medicine is one of the most valuable diagnostics and therapeutic methods in medicine. Its emersion from the beginning has been a compilation of important historical discoveries. The field of nuclear medicine has grown tremendously over the past 20 years. One of the most useful and unique applications of nuclear technology is the production of radiopharmaceuticals, which are undoubtedly revolutionary in medical science. Radiopharmaceuticals which are used for diagnostic imaging purposes are called radiotracers [14][1].

From a structural point of view radiopharmaceuticals include a radionuclide and a carrier molecule with high binding power or affinity able to bind to biological molecules in order to target particular organs, cells or tissues during the treatments or studies of the body [14].

The therapeutic uses of radiopharmaceuticals are more limited than the diagnostic applications. Radiation emitted by radiopharmaceuticals is widely used in cancer patients to kill cancer cells. The destruction of cancer cells is accomplished by ionization, so ionizing radiation with a short range is useful because this results in large amounts of tissue destruction in a small, confined area. The best isotopes for therapeutic purposes are those that emit low energy radiation like alpha or beta [15].

In radiopharmaceutical imaging, images of organs and tissues of interest can be presented by the scintigraphy process. It creates two-dimensional images and it functions based on radiotracer injection and distribution into tissues or bones which leads to formation of images. Consequently, images are obtained by a medical device known as gamma cameras that detects gamma rays [16]. On the other hand, SPECT and PET cameras produce three-dimensional images. Hence, they are classified as separate imaging techniques. Although, SPECT has lower detection sensitivity compared to PET [16].

PET and SPECT are often coupled with other imaging techniques such as Computed Tomography (CT) or Magnetic Resonance Imaging (MRI) which provide structural information [17][18].

CT scans were introduced to provide information about those elements which are more electron dense like bones. Whereas, MRI scans are applicable in sensitive organs which have more soft tissues. PET and SPECT scans have high sensitivity but relatively low resolution. They provide information about biological processes, these scans can be combined with CT or MRI to give more clear images, for example merging CT and PET

scans together (Figure 1) provides more vivid images with more details [17].

CT is a method for imaging by using radioactive x-rays many times and a variety of signals taken from different angles and processing them by computer which lead to a 3-D image [19]. CT scan provides information to have better diagnosis of different diseases, injuries and traumas followed by better treatments. This method is fast and widely available for physicians to use it for both normal and emergency cases [19].

MRI combination with PET or SPECT provides perfect resolution for soft tissues (Figure 1). This method has another advantage where the patient exposed to less radiation-dose [17].

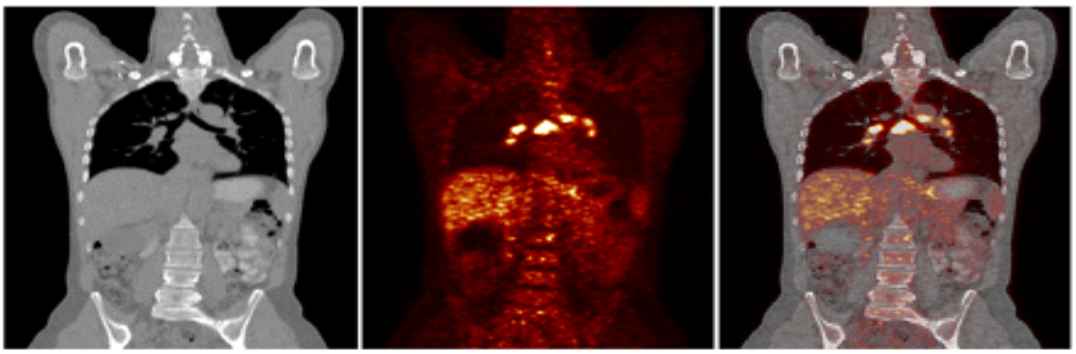

Figure 1. Attenuation map (left), PET images (middle), and fused PET/CT images (right) of patient with multiple [^{18}F]FDG–avid mediastinal and bihilar lymph node metastases.[20]

In nuclear medicine technetium-99m is an extensively used radioisotope with 89% abundance (Table 1) for diagnostics of several diseases such as some types of cancers. For example, bone metastasis is detectable by technetium-99m-Methylene Diphosphonate (MDP). [15]

Table 1. Physical Characteristics of Technetium-99m [21] *Abundance is the percent possibility of an emission type occurring with each decay

Mode of decay	Isomeric transition
Physical half-life	6 hours
Principal emissions (abundance)*	Gamma rays 140 keV (89%)

2.1.1 PET

Positron Emission Tomography (PET) is a cross-sectional imaging method. In PET short lived positron emitting radionuclides are being used that accumulate in certain places. PET cameras produce three-dimensional images to scan the biomarkers or tracers in the brain or in the other organs. The principle of this method consists of a positron (β^+) and an electron which have the same mass. Positron emitting radionuclides are produced by

cyclotrons via nuclear reactions. For example, production of fluorine-18 by oxygen-18 bombardment through $^{18}O(p,n)^{18}F$ nuclear reaction [22][1]. The unstable proton-rich nucleus decays eventually to the stable form. A nuclear proton is converted to a neutron and is accompanied by the emission of a β^+. Through the annihilation process, the β^+ and an electron collide with each other and consequently two gamma photons of 511 keV are generated travelling in opposite directions [23][24]. The gamma photons can be detected and collected by a ring of scintillation detectors [24]. A tracer like [^{18}F]FDG is injected to the body and it is consumed by the cancer cells which consume more glucose than normal cells. These tumor cells can be scanned by PET and they are shown brighter compare to the other tissues.[20]

2.1.2 *In vivo* imaging

PET radiopharmaceuticals are used in two ways of diagnosis: *in vivo* and *ex vivo.*
In vivo techniques are those in which a radiopharmaceutical enters the body of a living patient. Gamma radiation is released from the β^+ and electron annihilation passes through the body and is then received by radiation receivers and monitored to provide the desired information. This technique is highly sensitive, especially when coupled with CT or MRI. *In vivo* PET imaging is an invaluable diagnostic tool that is used around the world on a daily basis to diagnose patients, however it is also used in preclinical research studies. In preclinical PET laboratories healthy and diseased animals are studied to better understand diseases and to evaluate newly developed tracers [18][25].

2.1.3 *Ex vivo* imaging

Ex vivo diagnostic methods are those performed on samples of organs taken from a test animal like mice and rats. In order to perform *ex vivo* imaging for example on the brain, the animal is killed and the brain is imaged to get desirable resolution images. In order to study the distribution of the radiolabeled tracer in tissues taken from lab animals, a special molecular imaging technique is used which is known as autoradiography. Autoradiography facilitates finding the amount of the accumulated radioactivity in the cells [26]. In order to increase the sensitivity and dynamic range, digital autoradiography is being used recently that provides better sensitivity and linearity [27].

2.1.4 PET radionuclides and their production

PET radionuclides are synthetic positron-emitting radioisotopes that are produced by either nuclear reactors or particle accelerators such as cyclotrons depending on the application purpose and the type of nuclide. In the process of radionuclide production, a stable atom is converted to an unstable atom. These nuclear reactions are accomplished by bombarding a target nuclide with high energy particles such as protons or alpha particles [28][29]. Accelerators are the sources for charged particles like fast electrons (β), heavy charged particles (α), neutrons and protons in the MeV range [28][29].

Generally, cyclotrons are more attractive for medical science compared to nuclear reactors. Products from cyclotrons are suitable for nuclear medicine imaging like SPECT and PET scans and other studies since the ratio of β^+ particle and photon emission are high. Radionuclides produced by cyclotrons are generally have high Molar Activity (A_m) since the nuclear reactions usually produce a different element from the target material. Carrier free refers to those radionuclides having high A_m and the radioisotope of the element is in the pure form. In other word, the radionuclide has the abundance of 100% and the radioactive material does not contain the carrier. Examples of positron emitting radionuclides with short half-lives that are produced using a cyclotron are ^{11}C (20.4 min), ^{13}N (9.97 min), and ^{15}O (2.03 min). Another important positron emitting radionuclide is Fluorine-18 with the half-life of 109.8 min which is widely used for labeling the glucose analog, 2-deoxy-2-[^{18}F]fluoro-D-glucose ([^{18}F]FDG) [1][21][30].

The nuclear reactor is a large source of thermal neutrons. These neutrons can easily be absorbed by stable isotopes, the resulting isotope will have an additional neutron which increases mass number by one unit. The resulting isotope may be radioactive, meaning there is a radioisotope, or it may be stable. The production is not carrier free and the A_m is low. Examples of PET isotopes made this way are ^{32}P, ^{90}Y, ^{131}I, ^{188}Re and so on [31][28]. The maintenance of these reactors is challenging, and the maintenance costs are high [28][29].

^{18}F-Fluoride can be produced via the $^{18}O(p,n)^{18}F$ nuclear reaction by the irradiation of ^{18}O-enriched water with a 10-MeV proton beam from a cyclotron. The labeling with fluorine-18 will be discussed in the radiolabeling section [32][22].

For the production of Carbon-11, the $^{14}N(p,\alpha)^{11}C$ nuclear reaction is widely being used. Using a cyclotron, nitrogen gas is irradiated with a 10-MeV proton beam in the presence of O_2 or H_2 to generate [^{11}C]CO_2 or [^{11}C]CH_4 [33].

For carbon-11 labeling there two approaches known as Wet-chemistry approach and Gas-phase synthesis. Carbon-11 labeling will be discussed more in details later [34].

Table 2. Common positron emitting radionuclides [21]

Isotope	Half-life ($T_{1/2}$)	Max β^+ Energy (MeV)	β^+ Emission (%)	Target material and Natural abundance	Nuclear reaction
^{11}C	20.4 min	0.96	99.8	^{14}N (99.6%)	$^{14}N(p, \alpha)^{11}C$
^{13}N	10.0 min	1.19	100	^{16}O (99.76%)	$^{16}O(p,\alpha)^{13}N$
^{15}O	2.07 min	1.73	100	^{15}N (0.4%)	$^{15}N(p,n)^{15}O$
^{18}F	109.4 min	0.63	97.0	^{18}O (0.2%)	$^{18}O(p,n)^{18}F$
^{68}Ga	68.2 min	1.89	89.3	Gen (^{68}Ge), ^{68}Zn(18.5%)	$^{68}Zn(p,n)^{68}Ga$ $^{66}Zn(\alpha,2n)^{68}Ge$
^{64}Cu	12.8 h	0.65	17.4	^{64}Ni (0.9%)	$^{64}Ni(p,n)^{64}Cu$
^{76}Br	16.2 h	3.98	57.0	^{76}Se (9.1%)	$^{76}Se(3He,xn)^{76}Br$
^{89}Zr	3.27 d	0.90	22.7	^{89}Y (100%)	$^{89}Y(p,n)^{89}Zr$
^{124}I	4.18 d	2.13	25.0	^{124}Te (4.8%)	$^{124}Te(d,2n)^{124}I$

2.1.5 Radiolabeling

Radiolabeling refers to a chemical reaction in which a radionuclide is introduced to the target molecule. In the manufacture of any labeled radiopharmaceutical, there should be a compromise between the chemical yield and the radioactive decay. Therefore, any radiopharmaceutical must be synthesized, purified and analyzed during the half-life of the radionuclide [32][1].

Radiochemical yield (RCY) refers to the amount of product activity relative to the starting radioactivity and is normally reported as a percentage. Later, the radiolabeled drugs can be utilized by injection to the patient's body, inhalation or even orally [32].

As it was mentioned earlier, some practical radionuclides with short half-lives and high β^+ decay ratio such as ^{11}C, ^{15}O, ^{13}N, and ^{18}F are used in PET radiopharmaceuticals. Radionuclides like fluorine-18 and carbon-11 have many significant advantages in

radiopharmaceutical field. Hence, there are different types of reactions for carbon-11 and fluorine-18 labeling [28].

In fluorine-18 radiolabeling there are two direct labeling methods for fluorination: Nucleophilic $[^{18}F]F^-$ and Electrophilic $[^{18}F]F_2$ [32].

For ^{18}F-radiolabeling, there are two cyclotron production methods which are carrier added to generate either $[^{18}F]F_2$ gas. The first method is via $^{20}Ne(d,\alpha)^{18}F$ nuclear reaction [35] and the second method is "2-shoot method" using the $^{18}O(p,n)^{18}F$ nuclear reaction on a $^{18}O_2$ gas target [36] with a subsequent isotope exchange reaction with fluorine gas which leads to low A_m product. To reduce the carrier amount, the post-target production method for $[^{18}F]F_2$ was developed by Bergman and Solin [37] with high A_m starting from aqueous $[^{18}F]F^-$.

The low A_m, low specificity and low yield are some of the disadvantages of electrophilic fluorination, although; there are still radiopharmaceuticals which are prepared using electrophilic fluorination such as $[^{18}F]$fluoro-L-DOPA [32][38].

For nucleophilic fluorination, aqueous $[^{18}F]F^-$ is produced with the same $^{18}O(p,n)^{18}F$ nuclear reaction explained in electrophilic fluorination. ^{18}O-enriched water is irradiated with protons from a cyclotron. In nucleophilic fluorination A_m is high and $[^{18}F]$FDG is produced via this method [32] (Scheme 1).

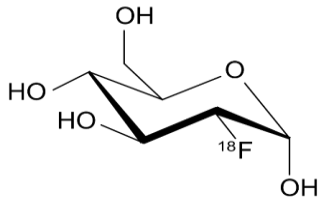

Scheme 1. $[^{18}F]$-FDG molecule

2.2. Carbon in chemistry

Carbon is a non-metal light element and it can be found almost everywhere in nature. It is the element of life and the human body is made up of 20% of carbon by joining other elements like Oxygen and Hydrogen. Carbon can be found in a various allotropic forms including graphite, diamond, amorphous carbon and graphene which are the most known structures, additionally, in room temperature carbon remains in its solid state. Through different synthetic routes, carbon can be changed into multiple structures. These diverse structures have their own properties.

Carbon has fifteen known isotopes with atomic masses between ^{8}C - ^{22}C. The least stable of these isotopes is carbon-8 with a half-life of 2.0 x 10^{-21} seconds [21].

Naturally occurring carbon isotopes have three forms. Carbon-12 consists of 6 protons and 6 neutrons. Over 98 % of carbon on our planet is carbon-12 and the rest are other isotopic forms of carbon [21]. Carbon-13 is the heaviest stable isotope. Carbon-14 is a rare unstable isotope and has eight neutrons and it is the only radioactive isotope of carbon found in nature, and it will decay by beta emission overtime to nitrogen-14 [21].

Carbon-11 is the radioisotope of carbon consisting of 6 protons and 5 neutrons that decays 99% by β^+ emission and 0.2% by electron capture to boron-11 as shown in Table 3. It is one of the most used radioisotopes in PET [21].

Table 3. Nuclei and relative abundance of Carbon isotopes and masses in Dalton [21]

Isotope	Mass(Da)	Natural Abundance (%)	Half-life ($T_{1/2}$)	Decay mode
^{11}C	11.01143	-	20.36 min	Electron capture, β^+
^{12}C	12.0	98.890	Stable	-
^{13}C	13.003355	1.110	Stable	-
^{14}C	14.003241	0.001	5730 Y	β^-

2.2.1. Carbon-11 radionuclide and its chemistry

In novel radiopharmaceutical development many factors are needed to be considered from radionuclide and labeling position selection to the precursor synthesis and labeling route [39].

Carbon-11 is one of the most useful radionuclides and one reason for this is that the introduction of carbon-11 into a biologically active molecule, does not affect the biochemical properties of the whole compound. Carbon-11 is commonly produced via the $^{14}N(p,\alpha)^{11}C$ nuclear reaction. $[^{11}C]CO_2$ and $[^{11}C]CH_4$ can be formed in the cyclotron target chamber, by adding oxygen and hydrogen to the target gas [39].

$[^{11}C]CO_2$ is the more functional of the two primary labeling precursors. $[^{11}C]CO_2$ can react with primary amines, organolithium, organomagnesium compounds [40]. For example, preparation of $[^{11}C]$acetone by the reaction of $[^{11}C]CO_2$ with methyl lithium [41].

Carbon chemistry provides much information to be used when developing carbon-11 radiosynthetic methods. The short half-life of carbon-11 has both pros and cons at the same time. The short half-life of carbon-11 provides an opportunity to have *in vivo* studies and allows more injections on a patient or animal on the same day. On the other hand, the short half-life of carbon-11 makes some limitations for production and transportation of the ^{11}C-labeled radiopharmaceuticals and short study frame [39].
Despite these limitations numerous radiolabeled molecules have been developed using the carbon-11 radionuclide [39].

2.2.2. CH_3I

In Carbon-11 chemistry, the most regular method for methylation is to use methylation agents like methyl iodide (MeI) and methyl triflate (MeOTf) which are derived from primary labeling precursor [^{11}C]CO_2. [^{11}C]MeI is the most frequently used secondary ^{11}C-labeling precursor but can be converted to the more reactive reagent [^{11}C]MeOTf.. The ^{11}C-methylation reaction can be implemented based on the vial approach or solid support approach [39]. The regent in the gas phase can either be mixed with the small amount of precursor in solution or be passed through a capillary loop the internal surface of which is coated with the precursor solution. [^{11}C]MeI can be used as an agent in the alkylation of carbanions and heteroatom nucleophiles which is the main application of this precursor, moreover, [^{11}C]MeI has been used recently as an electrophile in palladium reactions to form ^{11}C-C bonds which is a useful way for the labeling of substances with [^{11}C]methyl groups onto specific positions [42][34].
[^{11}C]MeI plays very important role for the formation of some other labeling precursors like L-and D-[methyl ^{11}C]-L-methionine [43] and [^{11}C]nitromethane [44].
[^{11}C]CO is applicable in the synthesis of carbonyl compounds and this labeling precursor is as important as [^{11}C]MeI for the syntheses of ^{11}C-labeled radiotracers [42].

2.2.3. [^{11}C]CH_3I Synthetic methods

There are two synthesis methods for [^{11}C]MeI, these are the “wet-chemistry” approach and the alternative method is the “gas phase” method which will be explained subsequently [34].

2.2.3.1. Wet-chemistry approach

In the wet method, cyclotron generated $[^{11}C]CO_2$ is reacted with lithium aluminum hydride ($LiAlH_4$) in dry THF or diethyl ether (Et_2O) and the reason to use THF or Et_2O is to trap and minimize the amount of incoming $[^{11}C]CO_2$. The solvent is then evaporated and a dry residue containing $[^{11}C]LiAl(OCH_3)_4$ is formed. Water is required to be added to the residue to hydrolyze and release $[^{11}C]MeOH$ as an intermediate product, $[^{11}C]MeOH$ is added in the presence of nitrogen gas to the refluxing hydriodic acid (HI) and $[^{11}C]MeI$ will be formed [45] (Scheme 2). In another reaction, HI 57% (aq) is added to the dry complex of lithium, $[^{11}C]MeI$ is formed from hydrolyzed $[^{11}C]MeOH$ [46].
Alternatively, hydrolyzed $[^{11}C]MeOH$ is distilled and collected in a U-tube containing diphosphorous tetraiodide (P_2I_4) and then heated [47].
Triphenylphosphine diiodide $(C_6H_5)_3PI_2$ can also be used instead of P_2I_4 with the same reaction condition with $[^{11}C]MeI$ as an end-product [48].
After producing $[^{11}C]MeI$ by any of the mentioned reactions, it is transported with the current of an inert gas through a drying column to the methylation vessel for tracer radiosynthesis. RCY is reliable in the wet method but using $LiAlH_4$ as a reducing agent has some disadvantages [42]. This reagent is a source of cold CO_2 which causes contamination and results in low A_m of $[^{11}C]MeI$, therefore, low A_m of final ^{11}C-labeled radiotracer. To have a high A_m of $[^{11}C]MeI$, the amount of $LiAlH_4$ should be reduced [49]. To trap $[^{11}C]CO_2$ tiny amount of ~5-7 µmoles $LiAlH_4$ would be enough to produce 74 –370 GBq at end of synthesis (E.O.S). 2M solution of $LiAlH_4$ in distilled THF gives ~2 µmoles of MeOH per ml [45]. The reduction of $[^{11}C]CO_2$ by $LiAlH_4$ is not easy especially when Et_2O is used as a solvent instead of THF in low temperature, EtOH is produced as a chemical impurity [49][34].
$[^{11}C]CO_2$ can be frozen in a small stainless steel loop, by submerging it in liquid Argon with the boiling point of -186 °C and then recovered from the trap by an inert gas (nitrogen or helium) flow as the loop is warmed to ambient temperature [50].
There were some arguments earlier about the components that affect the presence of non-radioactive elements and materials which cause low A_m of radiotracers labeled with carbon-11. A hint of THF can remain in $LiAlH_4$ after evaporation and this causes formation of MeOH and consequently CO_2. The amount of CO_2 thus formed can be reduced by decreasing the concentration of $LiAlH_4$/THF solution [58]. $LiAlH_4$ is the main source for carbon-12 contamination [52]. It is also believed that the contamination with non-radioactive carbon arises from the cyclotron process of $[^{11}C]CO_2$ production

[53][49]. Nowadays, it is clearly known that other factors can be sources of contamination such as quality of the reagents, target material, synthesis box, etc. and other system configuration of each site [42].

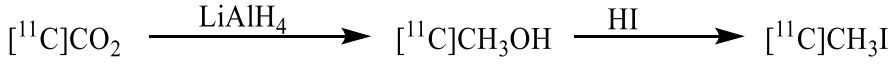

Scheme 2. Synthesis of [^{11}C]MeI via 'wet' method [43].

2.2.3.2. Gas-phase synthesis

Based on the difficulties and the low A_m in the wet method, another procedure known as gas-phase method was developed. This approach starts with [^{11}C]CH_4. [^{11}C]CH_4 can be produced in two ways. One is by $^{14}N(p,\alpha)^{11}C$ nuclear reaction in cyclotron using 5-10% H_2/N_2 target gas mixture in which A_m is high [54] . The other way is to start with [^{11}C]CO_2 which is produced in cyclotron and then converted to [^{11}C]CH_4 by the hydrogen reduction process in the presence of Ni catalyst (Scheme 3) [34] in recirculation procedure. [55][56].

This involves the reaction of [^{11}C]CH_4 in H_2 and Cl_2 gas with CrO_3 as a catalyst at 700 °C which results in formation of [^{11}C]CH_3OH. Followed by conversion of [^{11}C]CH_3OH to [^{11}C]MeI by passing it over $(C_6H_5)_3PI_2$ adsorbed on alumina at 160°C. RCY is satisfactory in this method, but the A_m is still low [57]. [^{11}C]MeI can also be formed from [^{11}C]CH_4 by a free radical iodination vapor reaction in the gas phase between 700-750 °C without using a catalyst [58][56]. The A_m values are higher of those in wet method.

Circulation process of gas-phase iodination is being performed to convert [^{11}C]CH_4 to [^{11}C]MeI. By using the Porapak trap and heating, the formed [^{11}C]MeI will be removed from the circulation process [59].

In another report [60] it is said that there are factors like I_2 concentration, flow rate through the reactor tube, reactor temperature and if any changes happens on one parameter, the others must be reoptimized so, [^{11}C]MeI yield will be maximized and [^{11}C]CH_2I_2 would be minimized under recirculation system starting with [^{11}C]CO_2 . With this method the RCY will be doubled.

By combining [^{11}C]CH_4 with iodine vapors in a non-thermal plasma reactor under low-pressure helium gas flow in a single-pass prototype device [^{11}C]MeI vapor will be released. By this method different free radicals and other ions are produced within the plasma and the reaction product selectivity is low [61].

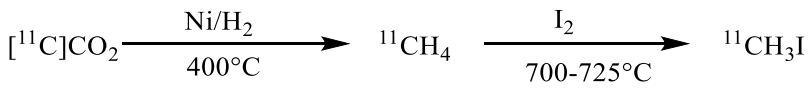

Scheme 3. Synthesis of [^{11}C]MeI via 'gas-phase' method [55][56]

There are some advantages of using gas-phase method compare to classic wet method to prepare [^{11}C]MeI. For instance, in the gas-phase method, since $LiAlH_4$ and HI are not used, there is lower contamination with carbon-12 which results in higher A_m and no need to do time consuming cleanings and dryings of the syntheses systems. When [^{11}C]CH_4 is produced in the target chamber, the highest radioactivity will be obtained [52].

Apart from the many benefits of using [^{11}C]MeI, there are a few drawbacks of using this methylation agent. In the wet method, using HI causes the vials and tubes getting rusted overtime and the apparatus must be changed, cleaned and dried frequently. Some PET radiotracers indicate low RCY when [^{11}C]MeI is used for heteroatom methylation reactions [42][62].

In these cases, more reactive [^{11}C]MeOTf can be used [42][62]. The reaction of [^{11}C]MeOTf is shown in scheme 4.

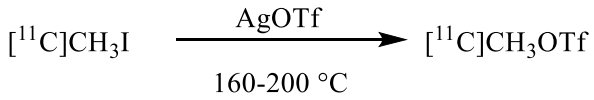

Scheme 4. Synthesis of [^{11}C]MeOTf from [^{11}C]MeI [63]

To put it in a nutshell, high A_m compounds labeled carbon-11 are formed by the ‘gas phase’ method. So, this method is chosen when the receptors require a high A_m tracer [42][34].

2.2.4. Radiochemistry application of Carbon-11

Radiotracers labeled with carbon-11 are applicable in early diagnosis of cancer [64], evaluation of the cancer treatment in therapeutic diagnostics [65], oncology imaging studies [66] and anticancer drug assessments [67]. Carbon-11 non-invasive PET studies are applicable to increase the therapeutic treatment results and identify those patients with metastatic disease [68].

There is a substitution process in which the nonradioactive element is replaced by its radioactive isotope in a biologically active tracer molecule without changing the biological properties. This process is called Hot-for-Cold substitution. In the case of

carbon element, carbon-11 is a substitute for carbon-12 in radiotracers labeled with carbon-11 [68]; some examples are [^{11}C]acetate as a biomarker for fatty-acids [69], and [^{11}C]choline as a marker for the synthesis of plasma membrane for the patients with neuroendocrine tumors [70]. Carbon-11 tracers are being used for imaging amino-acid transport for the patients with central nervous system (CNS) tumors [68].
Carbon-11 tracers are also applicable for imaging other diseases and organs. [^{11}C]acetate PET imaging in renal [71] and pancreas [72] diseases. [^{11}C]choline for prostate cancer diagnosis [73] [^{11}C]methionine in lung cancer [74] and [^{11}C]etomidate and [^{11}C]metomidate for imaging of the adrenal cortex and its tumors [75] are only some of the examples of carbon-11 tracers in PET imaging.

2.3. The Mitochondrial Translocator Protein (TSPO)

TSPO 18 kDa, is a transmembrane protein [4] that shows the activation of monocytic lineage cells including microglia and macrophages during neuroinflammation [76]. TSPO is incorporated with other mitochondrial channels and regulates their activities like voltage-dependent anion channel (VDAC) and the inner membrane anion channel (IMAC) [5]. The TSPO monomer consists of five transmembrane domains while the whole molecule has dimeric quaternary structure and it can be found in steroidogenic tissues like brain, kidney and heart cells [77][78]. Other forms of TSPO molecule are monomeric and oligomeric [79]. TSPO works as a regulator of cholesterol transport [80] to the nucleus that is related to the cell proliferation [80] in the human body.
TSPO was formerly called Peripheral Benzodiazepine Receptor (PBR) [4] due to the 1977 discovery which showed the ability of this protein to bind benzodiazepine drugs outside of the CNS [81]. TSPO is highly available in steroid synthesizing cells [82][83]. Oncologic, endocrine, neuropsychiatric and neurodegenerative diseases are some of the clinical applications of TSPO modulation [5][7].
Overexpressed TSPO acts as a target to detect neuroinflammation for PET ligands. TSPO PET imaging is a method for early diagnostics and theragnostic for CNS disorders [84].

2.3.1. Neuroinflammation

Inflammation of the nervous tissue or neuroinflammation is a defensive immune response against many types of trauma or toxins. This response is biologically complicated and includes signaling proteins and receptors. Neuroinflammation comes from many

responses from resident glial cells in CNS [85]. Neuroinflammation regulation is carried out by neuronal, glial, and endothelial cells within the neurovascular unit activity. The neurovascular unit acts as a platform to integrate pro-inflammatory and anti-inflammatory mechanisms. Inflammatory mediators including cytokines, chemokines, reactive oxygen species can be produced in the brain either by resident cells or cells migrating from the peripheral blood [86]. This procedure causes deterioration in blood-brain barrier (BBB) that affects the progress of local inflammation [87][88].

Microglia are macrophages in CNS which are derived from the mesoderm. Microglia moderate the neuron and blood vessel functions. When the BBB is healthy and there are no blood-born cells present, microglia and perivascular cells are the primary immune defense for the brain. [89]

In the condition that there is a neural injury or slight disorder in CNS environment, microglia react; coming up with faint physiological changes. This activation mode makes some changes in microglia morphology and leads them to the neuronal damage where release of proinflammatory molecules occurs. Microglia will be changed to the developed macrophages if the cells are dead. Due to this reason, they are called pathological sensor in the CNS [89].

Via two-photon microscopy, it is reported that resting microglia in healthy tissues frequently change their morphology due to processing, sampling and assessing the microenvironment. So, they are not passive all the time [90].

Microglial fast activation can happen without lymphocytic penetrations. This occurs in inflammatory brain disease known as multiple sclerosis (MS). The process elucidates neuroinflammation in different neurodegenerative disorders, such as AD, Parkinson's disease (PD) and Huntington disease (HD) [91].

2.3.2. Alzheimer's disease (AD)

According to The National Institute on Aging (NIA) which is the lead agency for AD research at the National Institutes of Health (NIH) located in the U.S, AD is now considered as a major health problem and defined as an advancing irreversible brain disease in which memory is damaged and after a while becoming more serious and results in dementia. Dementia is classified in the neurodegenerative disorders, symptoms such as memory impairment and mental deterioration make it difficult for the person to do routine functions. The damage happens in hippocampus where the memories form [92]. It normally happens to the elderly people who are in their 60s and over and some

individuals with down syndrome who are in their 50s. In rare cases, it may occur in middle-age between the ages of 30 to 60. There are some common symptoms like memory loss and language problems which may show differently in various patients. This disease is named after Dr. Alzheimer who found unusual changes in brain tissue of a patient which led to her death. He examined her brain and realized there are abnormal amyloid plaques and neurofibrillary tangles. The main reason for AD is amyloid plaques which can cause vascular dysfunction as well as affecting neuronal connectivity. Neurons are responsible for transferring messages from brain to organs and muscles. Consequently, when neuron cells die, other parts of the brain do not function appropriately. In the advanced level of this disease, brain tissue is considerably damaged and weakened [93][94].

Pathophysiology of AD starts some years before emersion of clinical symptoms, so it is possible to diagnose AD at early stages and essential to do so in order to control the progression. In this regard, [^{18}F]F-FDG-PET/CT (Figure 2) is a promising tool to detect not only tumors but also neuroimaging application for AD diagnosis. Due to the glucose cerebral metabolism and neuronal activity indicator, PET can discern AD over other causes of dementia. PET tracers correspond to β-amyloid deposition in the brain also and the example of this would be the [^{11}C]PiB [94][95] (Figure 2).

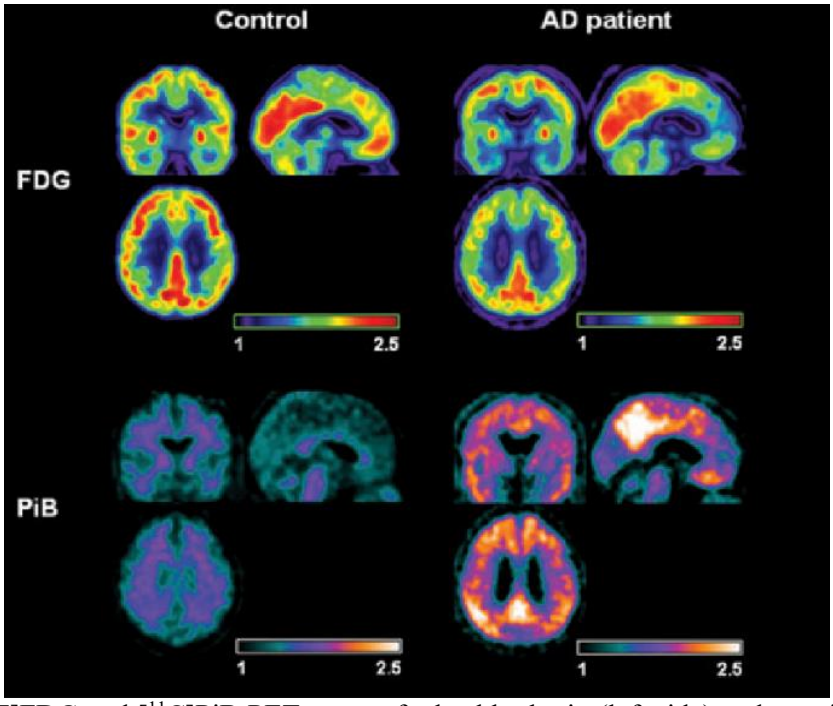

Figure 2. [^{18}F]FDG and [^{11}C]PiB PET scans of a healthy brain (left side) and a patient with AD (right side). In both scans, standardized uptake value ratios to the cerebellum are indicated using a color-coded scale (range: 1–2.5) [96].

2.3.3. PET tracers for TSPO and their applications in Neuroinflammation imaging

TSPO radioligands facilitate detection of neuroinflammatory disorders by PET. Some of these ligands are [^{11}C]PK11195, [^{11}C]PBR28, [^{18}F]DPA-714, [^{11}C]DPA-713 and the newest [^{18}F]F-DPA [97].

TSPO ligands can be used as diagnostic tools and many therapeutic applications to evaluate activation of microglia in human and animals [82].

[1- (2-chlorophenyl) -N - methyl -N- (1- methylpropyl)- 3- isoquinoline carboxamide] (PK11195) is a first-generation TSPO ligand (Scheme 5). It has been radiolabeled with carbon-11, and [^{11}C](R)-PK11195 is used in PET to image brain diseases and detect neuroinflammatory changes *in vivo* [98]. The [^{11}C](R)-PK11195 signal *in vivo* can be found in affected neural tracts and their cortical and subcortical areas. This ligand provides information about the progression of neuroinflammation and gives better understanding of brain disease and damage [92].

[^{11}C]PK11195 has poor signal-to-noise ratio [92] and high nonspecific binding, low brain uptake and high plasma protein uptake this results in not very accurate quantification [99].

Other second generation TSPO PET tracers have shown better results: for example [^{11}C]PBR28 (Scheme 6) which has been used for pre-clinical and clinical imaging overexpressed TSPO for the detection and quantification of neuroinflammation in brain regions [100]. Although [^{11}C]PBR28 is metabolized faster, it is more sensitive to detect neuroinflammation and TSPO overexpression in comparison with [^{11}C]PK11195 tracer [101].

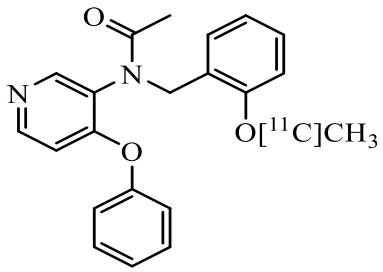

Scheme 5. [^{11}C](R)-PK11195 structure

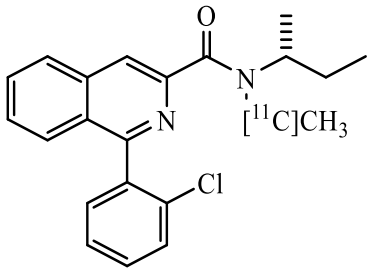

Scheme 6. [^{11}C]PBR28 structure

2.3.4. Pyrazolopyrimidine-type TSPO Ligands

In the following section second generation PET tracers for TSPO of the pyrazolopyrimidine-type are going to be discussed.

2.3.4.1. DPA-713 and DPA-714

N,N-diethyl-2-[2-(4-[^{11}C]methoxyphenyl)-5,7-dimethylpyrazolo[1,5-a]pyrimidin-3-yl]acetamide ([^{11}C]DPA-713) and N,N-diethyl-2-[2-(4-[^{18}F]fluoroethoxyphenyl)-5,7-dimethylpyrazolo[1,5-a]pyrimidin-3-yl]acetamide ([^{18}F]DPA-714) are promising second generation TSPO-PET radiotracers [102][103] (scheme 7).

In comparison between [^{11}C]DPA-713 and [^{11}C]PK 11195 they have similar brain uptake but [^{11}C]DPA-713 shows a better contrast of healthy and damaged brain, higher binding potential and higher signal-to-noise ratio since [^{11}C]DPA-713 has lower lipophilicity. So, it can be concluded that [^{11}C]DPA-713 is a suitable alternative to [^{11}C]PK 11195 as a tracer for PET of TSPO expression. DPA-713 ligand has an excellent specificity and binding affinity of $K_i = 4.7 \pm 0.2$ nM. [102].

[^{18}F]DPA-714 also has a high binding affinity of $K_i = 7$nM and low non-specific binding. A comparison between [^{11}C]PK11195 and [^{18}F]DPA-714 [104] shows that both TSPO tracers have similar brain uptake. Brain uptake value refers to the ability of drug transport across the BBB. In the case of [^{11}C]PK11195 and [^{18}F]DPA-714 brain uptake values are 3.3±1.2 %ID/g and 4.6±2.5 %ID/g respectively and [^{18}F]DPA-714 shows a significantly better signal-to-noise ratio. The advantage of using this tracer is due to its longer half-life of F-18 which enables the tracer to be distributed widely in the brain and its increased bioavailability in brain tissue makes [^{18}F]DPA-714 a suitable replacement for [^{11}C]PK11195. Furthermore, F-18 has low β^+ range and better image quality [104].

[^{11}C]-DPA-713 is more suitable for imaging mild inflammation. In addition, the fact that [^{18}F]-DPA-714 is an agonist PET tracer providing evaluation of different aspects of neuroinflammation [105].

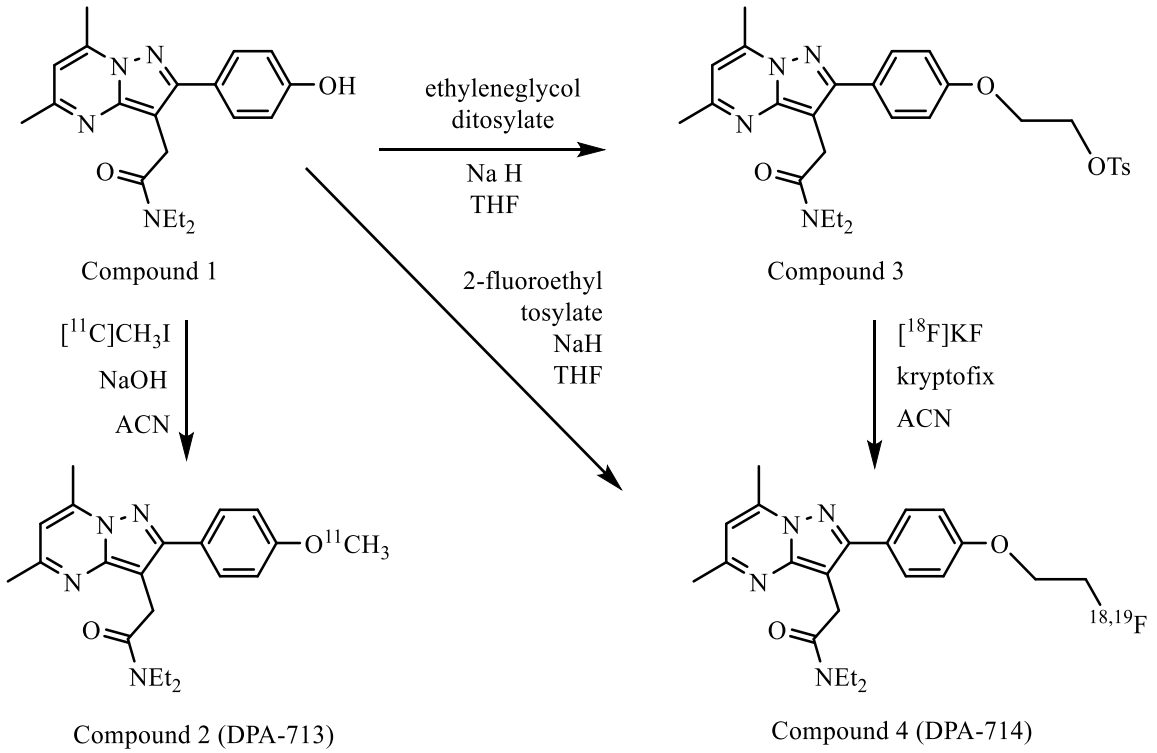

Scheme 7. Synthesis of [^{11}C]DPA-713 and [^{18}F]DPA-714 from the labeling precursor compounds 1 and 3 respectively [105].

2.3.4.2. F-DPA

TSPO ligands are developing considerably and new studies and results are constantly being published which indicates high potential for research in the area of TSPO radiotracers. In 2001 Selleri et al. [106] were looking into many different pyrazolopyrimidineacetamide ligands. They described a new TSPO ligand N,N-Diethyl-2-(2-(4-fluorophenyl)-5,7-dimethylpyrazolo[1,5-a]pyrimidin-3-yl)acetamide which had a high binding affinity of Ki = 9.2 ± 1.0 nM for TSPO.

In the recent years, new reports were published by Damont et al. [107] in 2015. They carried out a nucleophilic synthesis of [^{18}F]F-DPA by employing different precursors but the A_m was relatively poor.

Due to the difficulties in the nucleophilic labeling Keller et al. [9] employed electrophilic ^{18}F-fluorination for the synthesis of [^{18}F]F-DPA (Scheme 8). It was shown that [^{18}F]F-DPA is metabolically more stable than [^{18}F]DPA-714 and that [^{18}F]F-DPA has a quick entry into the brain [9]. [^{18}F]F-DPA has also successfully been applied to study neuroinflammation in a mouse model of AD [11].

Other research groups Wang et al. [12] and Zischler et al. [13] have developed nucleophilic ^{18}F-fluorination syntheses for [^{18}F]F-DPA with moderate A_m's. Wang et al. used a spirocyclic iodonium ylide as precursor and evaluated brain uptake of this tracer in a mouse model with AD and a rat model with ischemic stroke. Zischler et al. used a

boronic ester precursor and a novel method to prepare radiofluorinated [^{18}F]F-DPA (Scheme 9).

A considerable difference between [^{18}F]DPA-714 and [^{18}F]F-DPA is that there is no alkoxy linker to connect label and the aromatic ring [10].

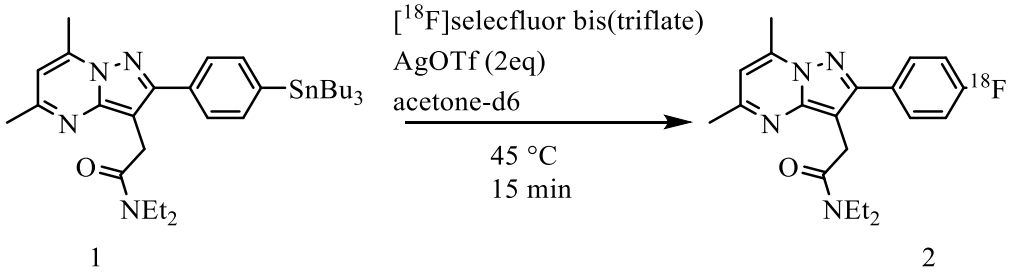

Scheme 8. Electrophilic synthesis of [^{18}F]F-DPA [9]

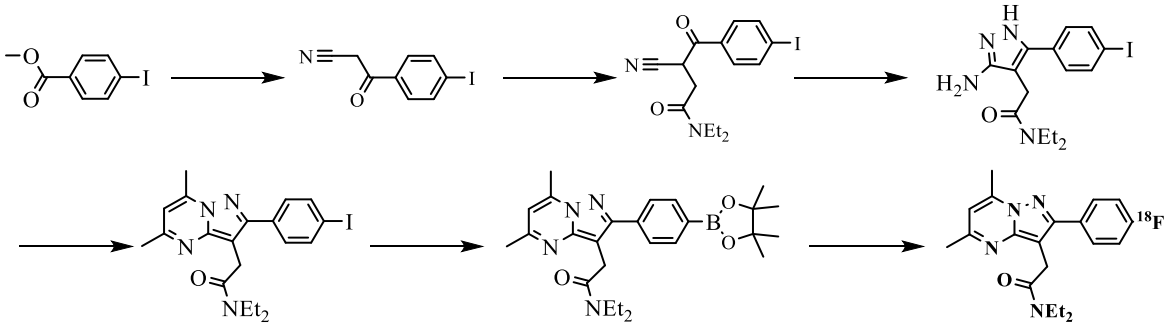

Scheme 9. Synthetic route of [^{18}F]F-DPA [13]

2.3.4.3. Me-DPA

In their article from 2001, Selleri et al. also described N,N-Diethyl-2-(2-(4-methylphenyl)-5,7-dimethylpyrazolo[1,5-a]pyrimidin-3-yl)acetamide (Me-DPA). This structure is an attractive potential tracer due to the binding affinity (Ki = 0.8 ± 0.1 nM) which is ten times more than that of F-DPA, (Ki = 9.2 ± 1.0 nM) [106]. Moreover, there is no restriction of carbon-11 labeling compared to nucleophilic and electrophilic fluorinations that makes the labeling process easier.

In this work, it is planned to make a boronic ester precursor which can be labeled with [^{11}C]-Me as shown in the scheme 10.

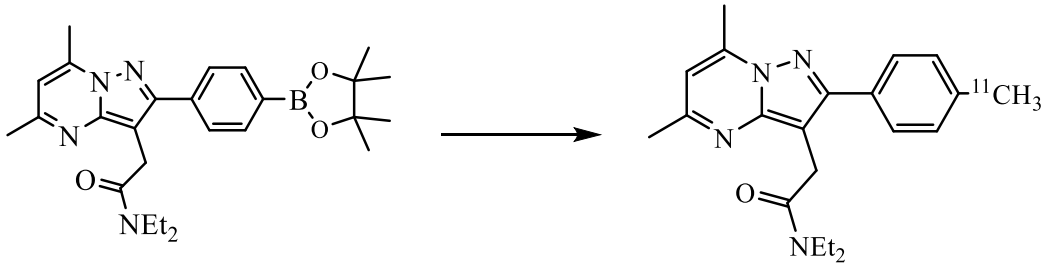

Scheme 10. Conversion of the boronic ester to [^{11}C]Me-DPA

3.Results

3-(4-Iodophenyl)-3-oxopropanenitrile

To produce pinacol boronic ester a synthesis with five steps was carried out. In the first step, 3-(4-Iodophenyl)-3-oxopropanenitrile was produced in 70% yield from methyl 4-iodobenzoate as starting material. As it can be observed from the ^{1}H NMR ($CDCl_3$, 500 MHz) 3-(4-Iodophenyl)-3-oxopropanenitrile, the aromatic protons are at 7.9 ppm (d, 2H, Ph) and 7.8 ppm (d, 2H, Ph) and methylene protons are at 3.9 ppm (s, 2H, CH_2CN). A tiny amount of THF might be present in the product.

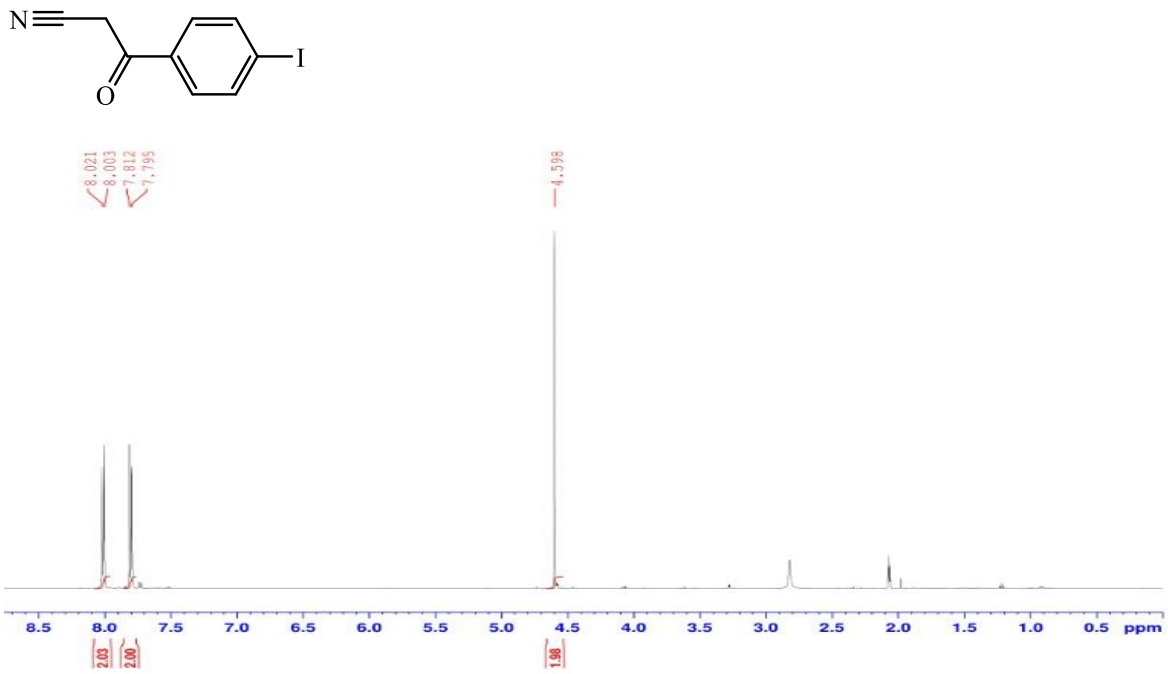

Figure 6. ^{1}H NMR ($CDCl_3$, 500 MHz) 3-(4-Iodophenyl)-3-oxopropanenitrile

3-Cyano-*N,N*-diethyl-4-(4-iodophenyl)-4-oxobutanamide

In the second synthesis step, 3-Cyano-N,N-diethyl-4-(4-iodophenyl)-4-oxobutanamide was produced from the 3-(4-Iodophenyl)-3-oxopropanenitrile in 70% yield. As it can be observed from the ^{1}H NMR ($CDCl_3$, 500 MHz) 3-Cyano-*N,N*-diethyl-4-(4-iodophenyl)-4-oxobutanamide, the aromatic protons are at 7.9 ppm (d, 2H, Ph) and 7.7 ppm (d, 2H, Ph), a methine proton is at 4.9 ppm (dd, 1H, CHCN), the methylene protons are at 3.4 – 3.3ppm (m, 5H, NCH_2, $COCH_2$) and 2.89 ppm (dd, 1H, $COCH_2$), the methyl protons are at 1.27 ppm (t, 3H, CH_3) and 1.1 ppm(t, 3H, CH_3). The product is pure enough to continue to the next synthesis.

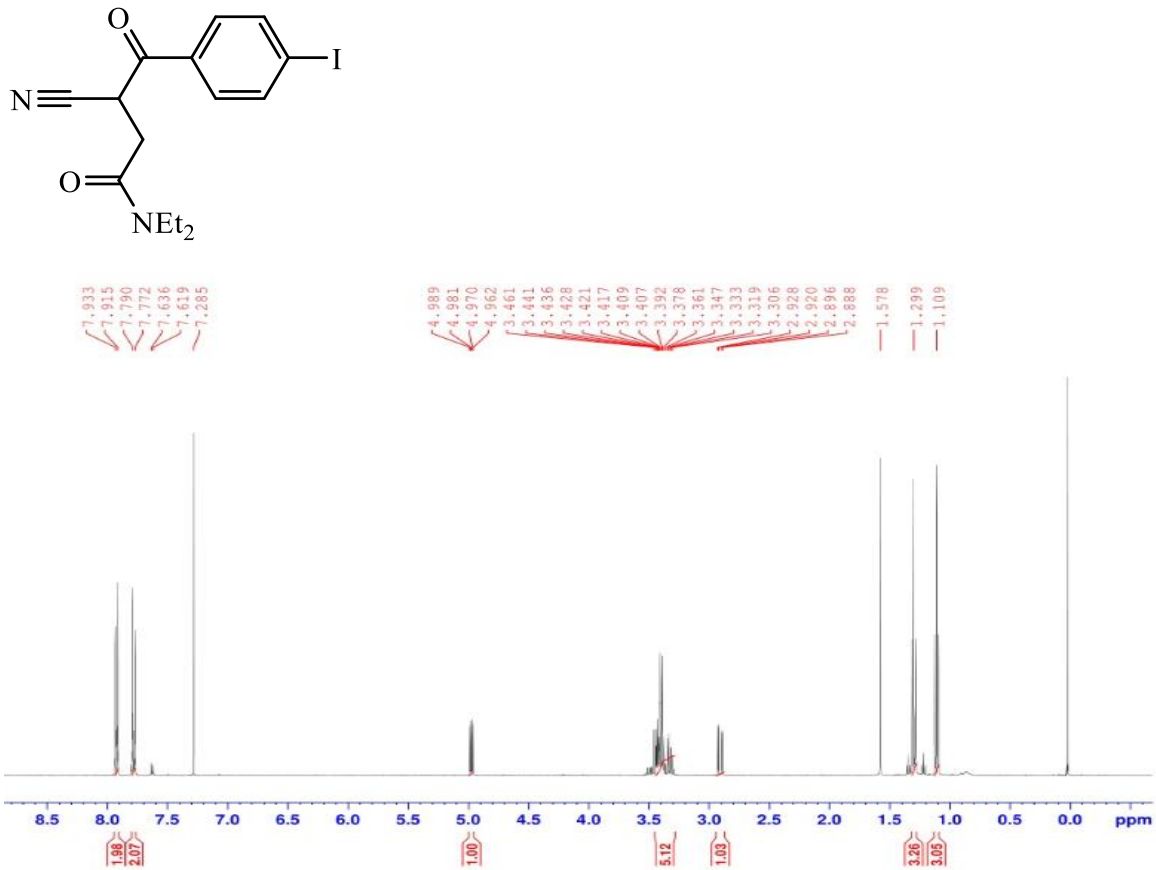

Figure 7. ^{1}H NMR ($CDCl_3$, 500 MHz) 3-Cyano-*N,N*-diethyl-4-(4-iodophenyl)-4-oxobutanamide

2-(3-Amino-5-(4-iodophenyl)-1H-pyrazol-4-yl)-*N,N*- diethylacetamide)

In the third synthesis step, 2-(3-Amino-5-(4-iodophenyl)-1H-pyrazol-4-yl)-N,N-diethylacetamide) is produced from the starting material 3-Cyano-N,N-diethyl-4-(4-iodophenyl)-4-oxobutanamide in 52% yield. As ^{1}H NMR ($CDCl_3$, 500 Mhz) 2-(3-Amino-5-(4-iodophenyl)-1H-pyrazol-4-yl)-*N,N*- diethylacetamide) indicates the aromatic benzene protons are at 7.7 ppm (d, 2H, Ph) and 7.1 ppm (d, 2H, Ph), the methylene protons are at 3.5 ppm (s, 2H, $COCH_2$), 3.3 ppm (q, 2H, $COCH_2$) and 3.1 ppm (q, 2H, NCH_2), the methyl protons are at 1.1 ppm (t, 3H, CH_3) and at 1 ppm (t, 3H, CH_3). The NMR shows pure product.

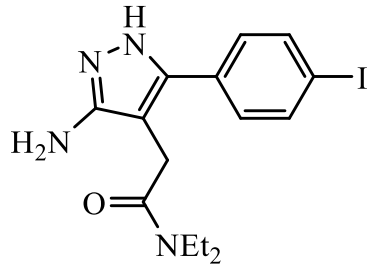

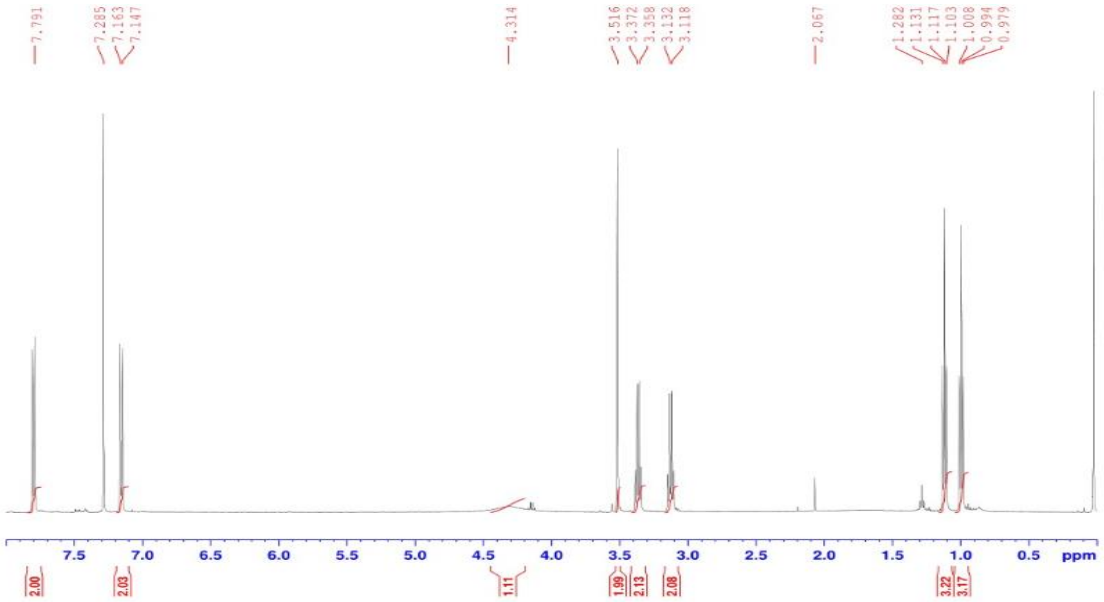

Figure 8. ^{1}H NMR ($CDCl_3$, 500 MHz) 2-(3-Amino-5-(4-iodophenyl)-1H-pyrazol-4-yl)-*N,N*- diethylacetamide)

N,N-Diethyl-2-(2-(4-iodophenyl)-5,7-dimethylpyrazolo[1,5-a]-pyrimidin-3-yl)acetamide

In the fourth synthesis step, N,N-Diethyl-2-(2-(4-iodophenyl)-5,7dimethylpyrazolo[1,5-a]-pyrimidin-3-yl) acetamide is produced in 95% yield from the 2-(3-Amino-5-(4-iodophenyl) -1H-pyrazol-4-yl)-N,N- diethylacetamide) as the starting material. As it can be induced from ^{1}H NMR ($CDCl_3$, 500 MHz) N,N-Diethyl-2-(2-(4-iodophenyl)-5,7-dimethylpyrazolo[1,5-a]-pyrimidin-3-yl)acetamide, the aromatic benzene protons are at 7.7 ppm (d, 2H, Ph) and 7.6 ppm (d, 2H, Ph), 4-pyrimidine proton is at 6.5 ppm (s, 1H, CHCN), the methylene protons are at 3.9 ppm (s, 2H, $COCH_2$), 3.5 ppm (q, 2H, NCH_2) and 3.4 ppm (q, 2H, NCH_2), the methyl protons are at 2.7 ppm (s, 3H, $PhCH_3$), 2.5 ppm (s, 3H, $PhCH_3$), 1.2 ppm (t, 3H, CH_3) and 1.1 ppm (t, 3H, CH_3). The product has high purity.

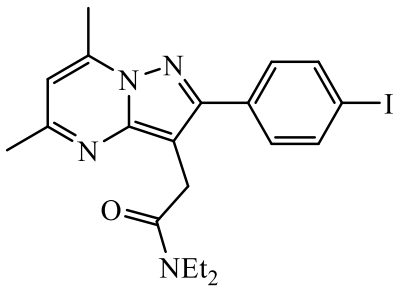

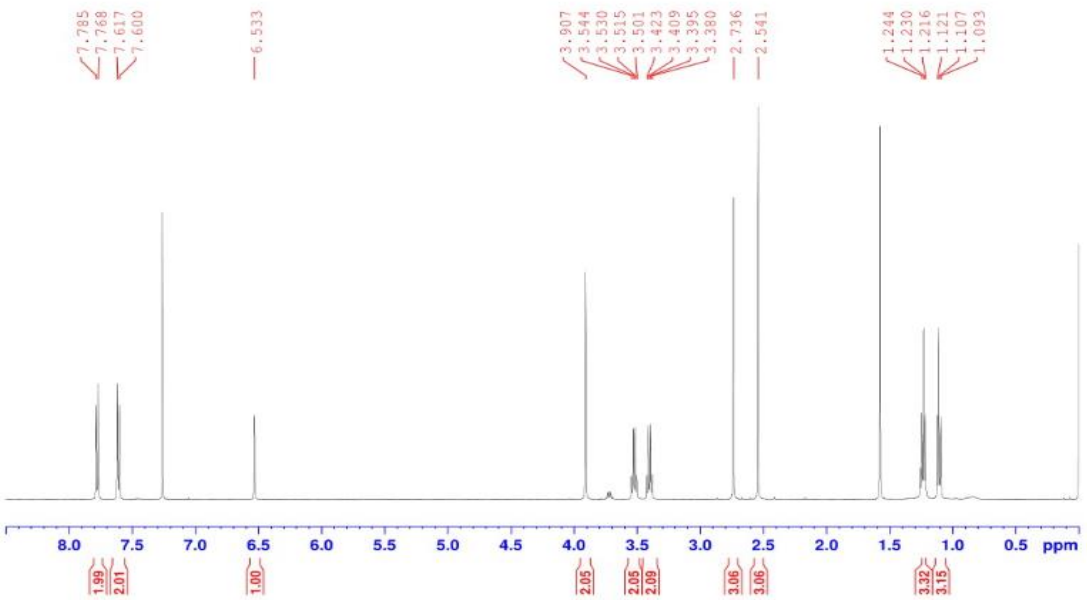

Figure 9. ^{1}H NMR ($CDCl_3$, 500 Mhz) N,N-Diethyl-2-(2-(4-iodophenyl)-5,7-dimethylpyrazolo[1,5-a]-pyrimidin-3-yl)acetamide

2-(5,7-dimethyl-2-(4-(4,4,5,5-tetramethyl-1,3,2-dioxaborolan-2-yl) phenyl)pyrazolo[1,5-a]pyrimidin-3-yl)-N,N-diethylacetamide

In the fifth synthesis step which leads to the pinacol boronic ester in 19% yield, N,N-Diethyl-2-(2-(4-iodophenyl)-5,7-dimethylpyrazolo[1,5-a]-pyrimidin-3-yl)acetamide is used as the starting material. Based on the NMR measurement from ^{1}H NMR ($CDCl_3$, 500 MHz) pinacol boronic ester, the aromatic benzene protons are at 7.89 ppm (d, 2H, Ph) and 7.83 ppm (d, 2H, Ph), 4-pyrimidine proton is at 6.5 ppm (s, 1H, CHCN), the methylene protons are at 3.95 ppm (s, 2H, $COCH_2$), 3.5 ppm (q, 2H, NCH_2) and 3.4 ppm (q, 2H, NCH_2), the methyl protons are at 2.7 ppm (s, 3H, $PhCH_3$), 2.5 ppm (s, 3H, $PhCH_3$), 1.3 ppm (s, 12H, CH_3), 1.2 ppm (t, 3H, CH_3) and at 1.1 ppm (t, 3H, CH_3).

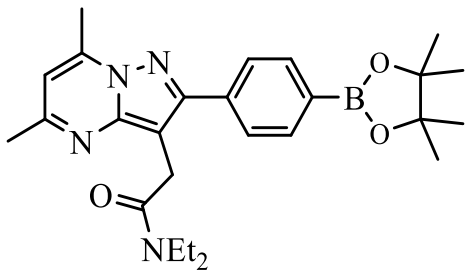

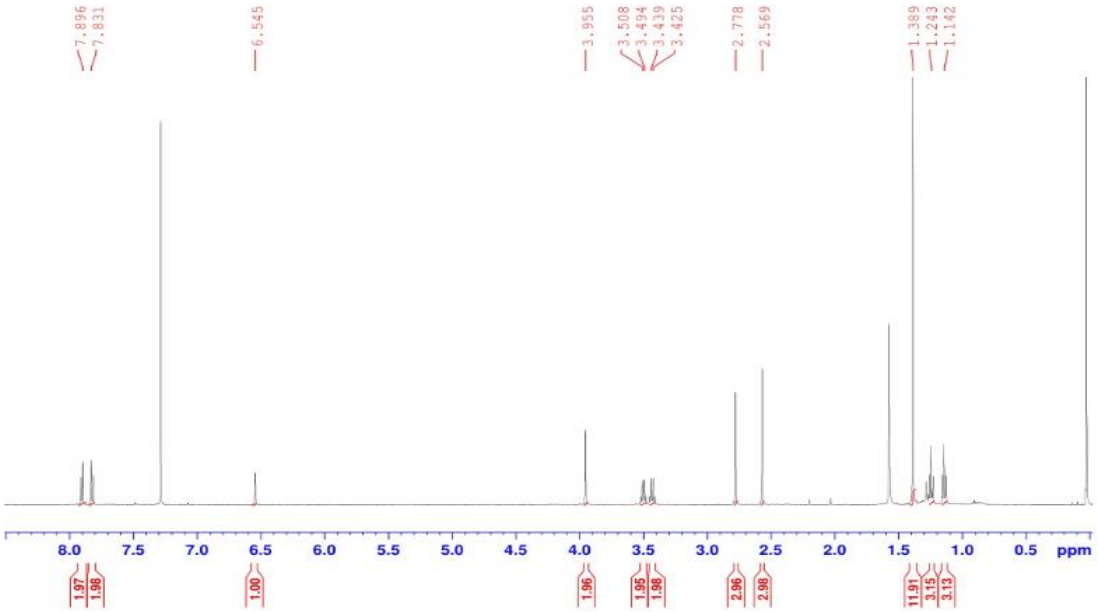

Figure 10. ^{1}H NMR (CDCl3, 500 MHz) pinacol boronic ester

4. Discussion

The aim of the presented work was to make a suitable precursor which can be labeled with carbon-11. There are factors affects the precursor selection such as stability, binding affinity, PH, thermal resistance and so on.

For this work, the boronic ester was chosen to synthesize as the precursor due to some reasons. First, boronic ester is a non-toxic compound compared to many other toxic organometallic precursors. Another advantage of this precursor is the stability of it for a long-term storage in comparison with the boronic acid. Boronic esters can be coupled with electrophiles, they can be used for reactions with nucleophiles; for example, the copper mediated fluorination, this makes them useful and versatile reagents. In this work 130 mg of the precursor was made. Although, the yield of the final reaction was low, and the final purification was challenging, enough precursor was prepared to perform the radiolabeling. The precursor will be used in radiolabeling with $[^{11}C]CH_3I$.

The purification challenges were due to the starting material and the product same retention time which caused using different eluents with variety of percentages.

Phenylboronic pinacol ester precursor was produced by Pd- catalyzed coupling reaction of B_2Pin_2 and adding N, N-Diethyl-2-(2-(4-iodophenyl)-5,7-dimethylpyrazolo[1,5-a]-pyrimidin-3 yl)acetamide in the presence of potassium acetate.

The boronic ester precursor can be used to synthesize both Carbon-11 and Fluorine-18 labeled PET tracers via $[^{11}C]$methylation, $[^{18}F]$fluoromethylation and nucleophilic and

electrophilic [^{18}F]fluorination.

Since boronic ester has higher lipophilicity compared to other boronic acid and lipophilic esters, the retention time is increasing and that results in better separation during tracer purification by HPLC.

In the future, the radiochemistry reaction and HPLC methods for analysis and purification will be developed.

5. Materials and methods

5.1. Precursor production

3-(4-Iodophenyl)-3-oxopropanenitrile

For the preparation of pinacol boronic ester the following method [107] was used.

In the first step 3-(4-Iodophenyl)-3-oxopropanenitrile was made. For this synthesis, a round bottom flask with a magnetic stirrer was placed in the cooling bath adding 50 mL of anhydrous THF to the flask by glass syringe while covering the flask by a septum in order to prevent any moisture or water entering to the flask and the synthesis must be carried out in dry condition. Then cooling bath was made by adding liquid nitrogen to MeOH. The temperature was kept at around -60 °C. 40 mL (100 mmol) n-butyllithium solution (2.5 M) in hexane was added the same way by glass syringe. Then 5.2 mL (100 mmol) CH_3CN in 50 mL of anhydrous THF was added to the flask slowly over 15-20 min while the temperature was below -50 °C. The mixture was stirred for 30 min at -60 °C. In another vial 12 g (45.8 mmol) methyl 4-iodobenzoate was dissolved in 70 ml of anhydrous THF and then added to the flask mixture over 20 min at -60 °C and after the addition, the reaction mixture was kept at the same temperature while stirring for 1 h. For the next 2 h the temperature was kept around -45 °C. After the mixing was completed. TLC monitoring was done to check if the reaction was completed. In order to quench the reaction, 200 ml of milli-Q water was added to the flask under vigorous stirring and the mixture was transferred to a beaker. Concentrated hydrochloric acid was added to the mixture to acidify the aqueous layer to pH 2. A white inorganic precipitate was formed and filtered by a funnel. The filtrate was extracted twice with EtOAc and washed twice with milli-Q water twice and once with brine. The organic phase was dried over sodium sulfate and filtered. Then organic phase was evaporated to dryness and the product was recrystallized from EtOAC as a purplish beige solid.

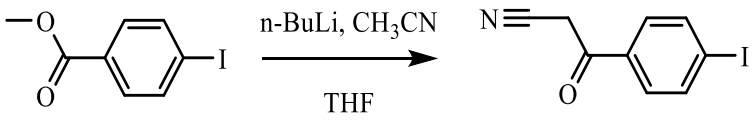

3-Cyano-N,N-diethyl-4-(4-iodophenyl)-4-oxobutanamide

In a flask with stirrer 0.285 g (7.085 mmol) of sodium hydroxide was added and dissolved in 35 mL EtOH and 6 mL of milli-q water. 1.757 g (6.5 mmol) of 3-(4-Iodophenyl)-3-oxopropanenitrile was added to the flask and stirred for 30 min at room temperature. 1.95 g (13 mmol) of sodium iodide was added to the mixture in one portion and dropwise addition of 0.99 mL (6 mmol) of N,N-diethylchloroacetamide to it. The reaction was stirred for 4 days at room temperature and monitored by TLC (Toluene / EtOAc 20%). The organic salt formed was removed by filtration under suction. The filtrate was evaporated to dryness. The purification was done by column chromatography with toluene/EtOAc 20% as an eluent. The starting material came out first and then the product with brownish beige color.

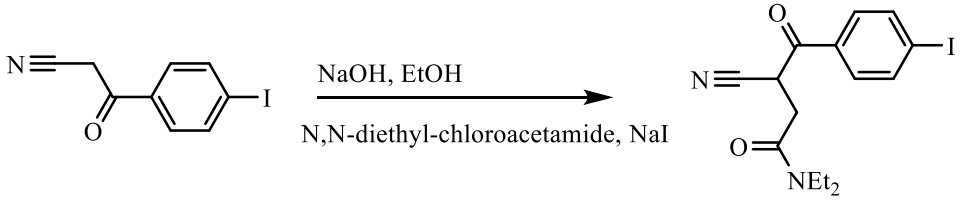

2-(3-Amino-5-(4-iodophenyl)-1H-pyrazol-4-yl)-*N,N*- diethylacetamide)

In the third step 2-(3-Amino-5-(4-iodophenyl)-1H-pyrazol-4-yl)-*N,N*- diethylacetamide) was made. To the 1.6g (4.2 mmol) of 3-Cyano-*N,N*-diethyl-4-(4-iodophenyl)-4-oxobutanamide in a flask was added 24 mL of EtOH followed by addition of 630 µL (12.9 mmol) of monohydrated hydrazine and 460 µL (7.7 mmol) of glacial acetic acid and it was placed in a bath oil with stirrer and a thermometer. The mixture was heated at reflux for 8 h while monitoring the progress by TLC. Then evaporated to dryness. The residue was extracted with EtOAC and water and basified by 3 M sodium hydroxide aqueous solution at pH 10. The organic layer was washed with water twice and brine, the organic layer was dried with sodium sulfate. Then it was filtered and concentrated to dryness by vacuum evaporator. The cold diethyl ether was added to the residue to collect solid particles, subsequently washed twice with cold diethyl ether followed by vacuum-drying. Eventually, the pure product was collected.

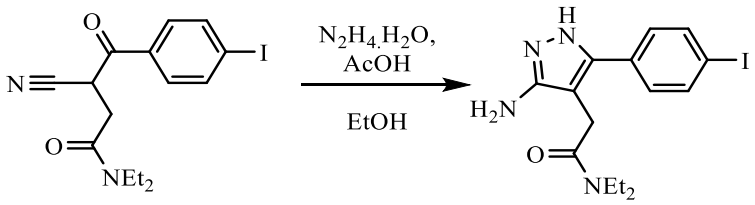

N,N-Diethyl-2-(2-(4-iodophenyl)-5,7-dimethylpyrazolo[1,5-a]-pyrimidin-3-yl)acetamide

In the fourth step, *N,N*-Diethyl-2-(2-(4-iodophenyl)-5,7-dimethylpyrazolo[1,5-a]-pyrimidin-3-yl)acetamide was made by adding 0.875 g (2.2 mmol) of 2-(3-Amino-5-(4-iodophenyl)-1H-pyrazol-4-yl)-*N,N*-diethylacetamide) in 17.5 mL of EtOH and 363 µL (28.2 mmol) of acetylacetone in a flask and placing that in an oil bath with a stirrer and thermometer. The reaction was stirred under reflux for 6 h and then cooled down to room temperature overnight. The pure product crystallized in the flask. The remaining organic phase was concentrated, and more product was collected by crystallization.

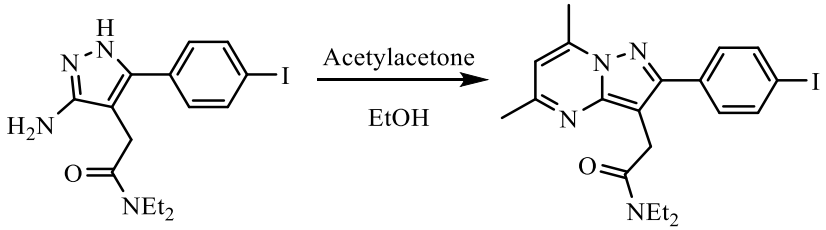

5.1.2. production of pinacol boronic ester

For the last step the pinacol boronic ester synthesis was done. 0.2 g (0.43 mmol) of N,N-Diethyl-2-(2-(4-iodophenyl)-5,7-dimethylpyrazolo[1,5-a]-pyrimidin-3-yl)acetamide, 35 mg (10 mol %) of [1,1′Bis(diphenylphosphino)ferrocene]dichloropalladium(II), 0.127 g (1.3 mmol) of Potassium acetate and 0.218 g (0.86 mmol) of *bis*(pinacolato)diboron (B_2Pin_2) were added to a small flask and covered by a septum to prevent any moisture to enter and 5 mL of dry toluene was added by syringe to it under the argon flow. The flask was purged with argon and placed in an oil bath with the stirrer and the thermometer. The mixture was heated up to reflux around 100 °C for 48 h. TLC monitoring was done.

The reaction mixture extracted with EtOAC, water and brine. The organic layers were dried with sodium sulfate, filtered, and evaporated to dryness. The product was purified by column chromatography with CH_3CN as eluent.

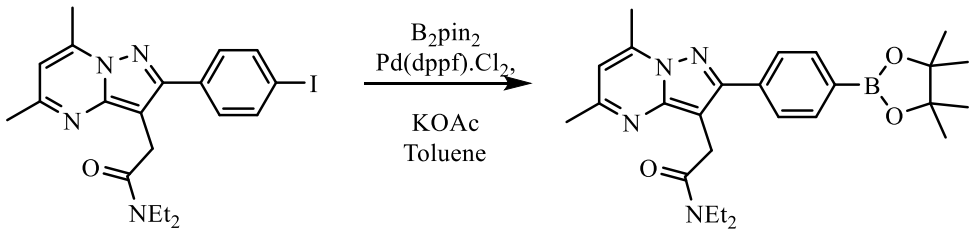

5.2. Characterization methods

5.2.1. Nuclear Magnetic Resonance (NMR) spectroscopy

The NMR instrument used in this project is Bruker 500 MHz (TYBruker500) for all the measurements. The temperature of instrument is set to 98 K. Approximately 750 µl of deuterated solvent was used for the NMR tube corresponding to 6 cm level of solvent.

5.2.2. Thin layer chromatography (TLC)

TLC chromatography was used to analyze the mixtures by separating the compounds. In this work, several TLC measurements during and after each synthesis and reactions.

5.2.3. Column chromatography

It is used for purification of compounds and consists of a column, silica gel and eluent which is called mobile phase. In this work, several purifications carried out on the second and fifth steps using different eluents and percentages.

6. Acknowledgement

This work is supported by Turku PET Centre radiochemistry research group Professor Olof Solin, Dr. Anna Kirjavainen and Dr. Thomas Keller and many thanks for their non-stop assists.

7. Abbreviation list

AD	Alzheimer's Disease
A_m	Molar activity
β^+	Positron
B_2Pin_2	Bis(pinacolato)diboron
BBB	Blood-brain barrier
CT	Computed Tomography
CH_2I_2	Diiodomathane
CH_3CN	Acetonitrile
$(C_6H_5)_3PI_2$	Triphenylphosphine diiodide
CNS	Central Nervous System
DPA-714	*N,N*-diethyl-2-[4-(2-fluoroethoxy)phenyl]-5,7-dimethylpyrazolo[1,5-a]pyrimidine-3-acetamide
DPA-713	*N,N*-diethyl-2-(4-methoxyphenyl)-5,7-dimethylpyrazolo[1,5-*a*]pyrimidine-3-acetamide
EtOAc	Ethyl acetate
EtOH	Ethanol
F-DPA	N,N-Diethyl-2-[4-fluorophenyl]-5,7-dimethylpyrazolo[1,5-*a*]pyrimidine-3acetamide
[^{18}F]FDG	2-[^{18}F]Fluoro-2-deoxy-2- D-glucose
[^{18}F]F^-	[^{18}F]Fluoride ion
HI	Hydroiodic acid
MeI	Methyl Iodide
MeOTf	Methyl triflate
MeOH	Methanol
MRI	Magnetic Resonance Imaging
NMR	Nuclear Magnetic Resonance
PBR	Peripheral benzodiazepine receptor
PK111195	[1-(2-chlorophenyl)-N-methyl-N-(1-methylpropyl)-3-isoquinoline carboxamide]

PET	Positron Emission Tomography
P_2I_4	Diphosphorous tetraiodide
RCY	Radiochemical yield
SPECT	Single - Photon Emission Computed Tomography
TSPO	18kDa Translocator Protein
TLC	Thin Layer Chromatography
THF	Tetrahydrofuran

8. References

1. Ruth TJ, "The uses of radiotracers in the life sciences", *Rep. Prog. Phys*., **2009**, 72, 1

2. Clifford Chao KS, Bosch WR, Mutic S, Lewis JS, Dehdashti F, Mintun MA, Dempsey JF, Perez CA, Purdy JA, Welch MJ, "A novel approach to overcome hypoxic tumor resistance: Cu-ATSM-guided intensity-modulated radiation therapy", *Int. J. Radiat. Oncol. Biol. Phys.,* **2001**, 49(4), 1171-1182

3. Papadopoulos V, Baraldi M, Guilarte TR, Knudsen TB, Lacapère J, Lindemann P, Norenberg MD, Nutt D, Weizman A, Zhang M, Gavish M, "Translocator protein (18kDa): new nomenclature for the peripheral-type benzodiazepine receptor based on its structure and molecular function." *Trends Pharmacol Sci*. **2006**, 27(8), 402-409

4. Anholt RR, Pedersen PL, De Souza EB, Snyder SH., "The peripheral-type benzodiazepine receptor. Localization to the mitochondrial outer membrane." *J Biol Chem*. **1986**, 261(2), 576-583.

5. Fujinaga M, Luo R, Kumata K, Zhang Y, Hatori A, Yamasaki T, Xie L, Mori W, Kurihara Y, Ogawa M, Nengaki N, Wang F, Zhang M-R, "Development of a ^{18}F-Labeled Radiotracer with Improved Brain Kinetics for Positron Emission Tomography Imaging of Translocator Protein (18 kDa) in Ischemic Brain and Glioma." *J. Med. Chem*. **2017**, 60(9), :4047-4061.

6. Taketani, S, Kohno H, Furukawa T, Tokunaga R, "Involvement of Peripheral-Type Benzodiazepine Receptors in the Intracellular Transport of Heme and Porphyrins" *J. Biochem*. **1995**, 117(4), 875-880.

7. James ML, Fulton RR, Vercoullie J, Henderson DJ, Garreau L, Chalon S, Dolle F, Costa B, Guilloteau D, Kassiou M, "DPA-714, a New Translocator Protein–Specific Ligand: Synthesis, Radiofluorination, and Pharmacologic Characterization." *J. Nucl. Med*. **2008**, 49(5), 814-822

8. Wu C, Yue X, Lang L, Kiesewetter DO, Li F, Zhu Z, Niu G, Chen X, "Longitudinal PET imaging of muscular inflammation using ^{18}F-DPA-714 and ^{18}F-Alfatide II and differentiation with tumors." *Theranostics*. **2014**, 4(5), 546-555.

9. Keller T, Krzyczmonik A, Forsback S, López-Picón FR, Kirjavainen AK, Takkinen J, Rajander J, Cacheux F, Damont A, Dollé F, Rinne JO, Haaparanta-Solin M, Solin O, "Radiosynthesis and Preclinical Evaluation of [^{18}F]F-DPA, A Novel Pyrazolo[1,5a]pyrimidine Acetamide TSPO Radioligand, in Healthy Sprague Dawley Rats" *Mol. Imaging. Biol.* **2017**, 19, 736–745

10. Keller T, López-Picón FR, Krzyczmonik A, Forsback S, K. Kirjavainen AK, Takkinen JS, Alzghool O, Rajander J, Teperi S, Cacheux F, Damont A, Dollé F, Rinne JO, Solin O, Haaparanta-Solin M, "[^{18}F]F-DPA for the detection of activated microglia in a mouse model of Alzheimer's disease", *J. Nucl. Med. Bio*. **2018**, 67, 1-9

11. Keller T, López-Picón FR, Krzyczmonik A, Forsback S, Takkinen JS, Rajander J, Teperi S, Dollé F, Rinne JO, Haaparanta-Solin M, Solin O, *J. Cereb. Blood Flow Metab.* **2020**, 40(5), 1012-1020

12. Wang L, Yao S, Tang R, Zhu H, Zhang L, Gong J, Chen Q, Lee Collier T, Xu H, Liang SH. "A concisely automated synthesis of TSPO radiotracer [^{18}F]FDPA based on spirocyclic iodonium ylide method and validation for human use", *J. Labelled Comp. Radiopharm.* **2020**, 63, 119–128

13. Zischler J, Kolks N, Modemann D, Neumaier B, Zlatopolskiy BD, "Alcohol-Enhanced Cu-Mediated Radiofluorination", *J. Chem.Photo.Chem*. **2016**, 23(14), 3251-3256

14. Eckelman WC, "The status of radiopharmaceutical research", *Nucl. Med. Biol.,***1991**, 18(7), iii-vi

15. Bhattacharyya S, Dixit M, "Metallic radionuclides in the development of diagnostic and therapeutic radiopharmaceuticals." *Dalton Trans*. **2011**, 40(23), 6112–6128

16. Keidar Z, Israel O, Krausz Y. "SPECT/CT in tumor imaging: technical aspects and clinical applications." *Semin Nucl Med*. **2003**, 33(3), 205-218

17. de Kemp RA, Epstein FH, Catana C, Tsui BMW, Ritman EL, "Small-animal molecular imaging methods." *J Nucl Med*. **2010**, 51 (5 Suppl), 18S-32S.

18. Wagenaar DJ, Kapusta M, Li J, Patt BE, "Rationale for the combination of nuclear medicine with magnetic resonance for pre-clinical imaging." *Technol Cancer Res Treat*. **2006**, 5(4), 343-350

19. Wijdicks, E.F.M. The First CT Scan of the Brain: Entering the Neurologic Information Age. *Neurocrit Care,* **2018**, 28, 273–275.

20. Martinez-Möller A, Souvatzoglou M, Delso G, Bundschuh RA, Chefd'hotel C, Ziegler SI, Navab N, Schwaiger M, Nekolla SG, "Tissue classification as a potential approach for attenuation correction in whole-body PET/MRI: evaluation with PET/CT data." *J Nucl Med*. **2009**, 50(4), 520-526.

21. International Atomic Energy Agency; Nuclear Data Section; A-1400 Vienna; Austria. Live Chart of Nuclides. (https://www-nds.iaea.org/relnsd/vcharthtml/VChartHTML) accessed: Jan-Oct 2019

22. Nickles RJ, Daube ME and Ruth TJ. An 18O2 target for the production of [18F]F2. *Int J Appl Radiat Isot*. **1984**; 35, 2, 117–122

23. Paans AM, van Waarde A, Elsinga PH, Willemsen AT, Vaalburg W., "Positron emission tomography: the conceptual idea using a multidisciplinary approach." *Methods*. **2002**, 27(3), 195-207.

24. Phelps ME, Hoffman EJ, Mullani NA, Ter-Pogossian MM. "Application of annihilation coincidence detection to transaxial reconstruction tomography." *J. Nucl. Med.* **1975**, 16, 210–24.

25. Brownell AL, Livni E, Galpern W, Isacson O., "In vivo PET imaging in rat of dopamine terminals reveals functional neural transplants." *Ann Neurol*. **1998**, 43(3), 387-390.

26. Schotte A, de Bruyckere K, Janssen PF, Leysen JE, "Receptor occupancy by ritanserin and risperidone measured using ex vivo autoradiography." *Brain Res*. **1989**, 500(1-2), 295-301.

27. Ott RJ, MacDonald J, Wells K, "The performance of a CCD digital autoradiography imaging system" *Phys. Med. Biol.* **2000**, 45, 2011

28. Volkert WA, Hoffman TJ. "Therapeutic radiopharmaceuticals." *Chem Rev*. **1999**, 99(9), 2269-2292.

29. Lagunas- solar, MC., et al., "Cyclotron production of PET radionuclides: ^{118}Sb from high-energy protons on natural Sb targets", *J. Nucl. Med. Biol*. **1990**,41(6), 521-529

30. Ido T, Wan C-N, Casella V, Fowler JS, Wolf AP, Reivich M, Kuhl DE, "Labeled 2-deoxy-D-glucose analogs. ^{18}F-labeled 2-deoxy-2-fluoro-D-glucose, 2-deoxy-2-fluoro-D-mannose and ^{14}C-2-deoxy-2-fluoro-D-glucose", *J. Lab. Camp. Radparm.* **1978**, 14(2), 175-183

31. Pervez S, Mushtaq A, Arif N, Chohan ZH, "^{188}Rhenium-EDTMP: A potential therapeutic bone agent." *J. Radioanalytical. Nucl. Chem.*, **2003**, 257, 417–420.

32. Hamacher K, Coenen HH, Hamacher K, "Efficient Stereospecific Synthesis of No-Carrier-Added 2-[^{18}F]-fluoro-2-deoxy-D-glucose Using Aminopolyether Supported

Nucleophilic Substitution", *J. Nucl. Med*. **1986**, 27, 235-238

33. Wagner R, Stöcklin G, Schaack W, "Production of carbon-11 labelled methyl iodide by direct recoil synthesis", *J. Label. Compd. Radiopharm*. **1981**, 18(11), 1557-1566

34. Kniess T, Rode K, Wuest F, "Practical experiences with the synthesis of [^{11}C]CH_3I through gas phase iodination reaction using a TRACERlabFXC synthesis module, *Appl, Radiat. Isotopes.* **2008**, 66(4), 482-488

35. Casella V, Ido T, Wolf AP, Fowler JS, MacGregor RR, Ruth TJ, "Anhydrous F-18 Labeled Elemental Fluorine for Radiopharmaceutical Preparation", *J. Nucl. Med*. **1980**, 21, 750-757

36. Nickels RJ, Daube ME, Ruth TJ, "An $^{18}O_2$ target for the production of [^{18}F]F_2", *Int. J. Appl. Radiat. Isotop.,* **1984**, 35(2), 117-122

37.Bergman J, Solin O, "Fluorine-18-labeled fluorine gas for synthesis of tracer molecules", *J. Nucl. Med. Biol.,* **1997**, 24(7), 677-683

38. de Vries EFJ, Luurtsema G, Brüssermann M, Elsinga PH, Vaalburg W, "Fully automated synthesis module for the high yield one-pot preparation of 6-[^{18}F]fluoro-L-DOPA," *Appl. Radiat. Isotopes.*, **1999**. 51(4), 389–394.

39. Dahl K, Halldin, C, Schou, M., "New methodologies for the preparation of carbon-11 labeled radiopharmaceuticals" *Clin Transl Imaging*, **2017**, 5, 275–289.

40. Scott PJH. "Methods for the incorporation of carbon-11 to generate radiopharmaceuticals for PET imaging." *Angew. Chem. Int. Ed.* **2009**, 48(33), 6001-6004.

41. Studenov AR, Berridge MS, Soloviev DV, Matarrese M, Todde S. "High yield synthesis of [^{11}C]-acetone through selective quenching of methyl lithium." *Nucl Med Biol*. **1999**, 26(4), 431-435.

42. Gomez-Vallejo V, Llop J, "Specific activity of [^{11}C]CH_3I synthesized by the ''wet'' method: Main sources of non-radioactive carbon", *Appl. Radiat. Isotopes*, **2009**, 67, 111–114

43. Långström B, Antoni G, Gullberg P, Halldin C, Malmborg P, Någren K, Rimland A, Svärd H, "Synthesis of L- and D-[methyl-^{11}C]methionine" *J. Nucl. Med*. **1987**, 28(6), 1037-1040.

44. Schoeps K-O, Halldin C, Stone-Elander S, Långström B, Greitz T, "Preparation of ^{11}C-nitromethane and an example of its use as a radiolabeling precursor",

J. Labelled. Comp. Radiopharm, **1988**, 25(7), 749-758

45. Marazano C, Maziere M, Berger G, Comar D, "Synthesis of methyl iodide-^{11}C and formaldehyde-^{11}C". *Int. J. Appl. Radiat. Isot*. **1977**, 28, 49-52.

46. Ehrenkaufer RLE, Morton T, Mach RH, Defilippi F, "Siemens/CTI/IBA automated system for production of [C-11]methyl iodide: Ongoing evaluation, operating parameters and field modifications". *J. Label Comp. Radiopharm*., **1995**, 37, 660-661.

47. Oberdorfer F, Hanisch M, Helus F, Maier-Borst W, "A new procedure for the preparation of ^{11}C-labelled methyl iodide". *Int. J. Appl. Radiat. Isot*. **1985**, 36(6), 435-438.

48. Holschback M, Schuller M, "An on-line method for the preparation of n.c.a. [$^{11}CH_3$]trifluoromethanesulfonic acid methyl ester", *Int. J. Appl. Radiat. Isot,* **1993**, 44(5), 897-898

49. Matarrese M, Soloviev D, Todde S, Neutro F, Petta P, Carpinelli A, Brussermann M, Kienle MG, Fazio F, "Preparation of [^{11}C] radioligands with high specific radioactivity on a commercial PET tracer synthesizer". *Nucl. Med. Biol*., **2003**, 30, 79-83.

50. Crouzel C, Långström B, Pike VW, Coenen HH, "Recommendations for a practical production of [^{11}C]methyl iodide." *Appl. Radiat. Isot*, **1987**, 38(8), pp. 601-603.

51. Iwata R, Ido T, Ujiie A, Takahashi T, Ishiwata K, Hatano K, Sugahara M, "Comparative study of specific activity of [^{11}C]methyl iodide: A search for the source of carrier carbon." *Appl. Radiat. Isot*, **1988**, 39(1), 1-7.

52. Zhang M-R, Suzuki K, "Sources of carbon which decrease the specific activity of [^{11}C]CH_3I synthesized by the single pass I_2 method." *Appl. Radiat. Isot*, **2005**, 62, 447-450

53. Ermert J, Stüsgen S, Lang M, Roden W, Coenen HH, "High molar activity of [^{11}C]TCH346 via [^{11}C]methyl triflate using the ''wet'' [^{11}C]CO_2 reduction method." *Appl. Radiat. Isot*. **2008**, 66, 619–624.

54. Helus F, Hanisch M, Layer K, Maier-Borst W, "Yield ratio of [^{11}C]–CO_2, [^{11}C]–CO and [^{11}C]–CH_4 from the irradiation of N_2/H_2 mixtures in the gas target." *J. Labelled Compd. Radiopharm*. **1986**, 23, 1195–1198.

55. Larsen P, Ulin J, Dahlstrøm K, Jensen M, "Synthesis of [^{11}C]iodomethane by iodination of [^{11}C]methane." *Appl. Radiat. Isot*., **1997**, 48(2), 153-157.

56. Link JM, Krohn KA, Clark JC, "Production of [^{11}C]CH_3I by single pass reaction of [^{11}C]CH_4 with I_2." *Nucl. Med. Biol*., **1997**, 24, 93-97.

57. Crouzel C, Fournier D, "N.C.A. gas phase production of [^{11}C]methanol from [^{11}C]methane: Application to the on line synthesis of [^{11}C]CH_3I." *J. Labelled Comp. Radiopharm.*, **1995**, 37, 9-80.

58. Larsen P, Ulin J, Dahlstrøm K. "A new method for production of labelled methyl iodide from ^{11}C-methane." *J. Labelled Comp. Radiopharm*., **1995**, 37, pp. 73-75.

59. Mock BH, Mulholland GK, Vavrek MT, "Convenient Gas Phase Bromination of [^{11}C]Methane and Production of [^{11}C]Methyl Triflate" *Nucl. Med. Biol*. **1999**, 26, 467–471

60. O'Neil JP, Powell J, Janabi M, "Evolution of a high yield gas phase $^{11}CH_3I$ rig at LBNL." *J. Labelled Comp. Radiopharm*., **2011**, 54 (Supplement 1), S101.

61. Eriksson J, Ulin J, Långström B. "[^{11}C]methyl iodide from [^{11}C]methane and iodine using a non-thermal plasma method." *J. Labelled Comp. Radiopharm*. **2006**, 49, 1177-1186.

62. Taddei C, Gee A, "Recent progress in [^{11}C]carbon dioxide ([^{11}C]CO_2) and [^{11}C]carbon monoxide ([^{11}C]CO) chemistry," *J. Labelled. Comp. Radiopharm*, **2017**, 61(3), 237-251

63. Jewett DM. "A simple synthesis of [^{11}C]methyl triflate." *Int J Rad Appl Instrum A*. **1992**, 43(11), 1383-1385.

64. Christman D, Crawford EJ, Friedkin M, Wolf AP, "Detection of DNA synthesis in intact organisms with positron-emitting (methyl-^{11}C)thymidine." *Proc Natl Acad Sci U S A*. **1972,** 69(4), 988-992.

65. Lindholm P, Leskinen-Kallio S, Minn H, Bergman J, Haaparanta M, Lehikoinen P, Någren K, Ruotsalainen U, Teräs M, Joensuu H, "Comparison of fluorine-18-fluorodeoxyglucose and carbon-11-methionine in head and neck cancer." *J Nucl Med*. **1993**, 34(10), 1711-1716.

66. Nozaki K, Kawai T, Fujimura T, Matsui H, Teshima T, Oshina T, Takahashi A, Sato Y, Yamada D, Azuma T, Hotta M, Nakajima K, Nakayama H, Minamimoto R, Kume H, "Carbon 11-choline positron emission tomography/computed tomography and palliative local therapy for castration-resistant prostate cancer." *Int Urol Nephrol*. **2019,** 51(10), 1763-1769.

67. Ravert HT, Klecker RW, Collins JM, Mathews WB, Pomper MG, Wahl RL, Dannals RF, "Radiosynthesis of [^{11}C]paclitaxel." *J. Label. Comp. Radiopharm*., **2002**, 45(6), 471-477.

68. Tu Z, Mach RH, "C-11 Radiochemistry in cancer imaging applications", *J. Curr. Top. Med. Chem.*, **2010**, 10, 1060-1095

69. Derlin T, Habermann CR, Lengyel Z, Busch JD, Wisotzki C, Mester J, Pávics L, "Feasibility of ^{11}C-Acetate PET/CT for Imaging of Fatty Acid Synthesis in the Atherosclerotic Vessel Wall", *J. Nucl. Med.*, **2011**, 52(12). 1848-1854

70. Hara T, Kosaka N, Shinoura N, Kondo T, "PET Imaging of Brain Tumor with [methyl-^{11}C]Choline", *J. Nucl. Med*. **1997**, 38, 842-847

71. Shreve P, Chiao PC, Humes HD, Schwaiger M, Gross MD, "Carbon-11-acetate PET imaging in renal disease." *J Nucl Med*. **1995**, 36(9), 1595-1601.

72. Shreve PD, Gross MD, "Imaging of the pancreas and related diseases with PET carbon-11-acetate." *J. Nucl. Med.,* **1997**, 38(8), 1305-1310

73. Kotzerke J, Prang J, Neumaier B, Volkmer B, Guhlmann A, Kleinschmidt K, Hautmann R, Reske SN, "Experience with carbon-11 choline positron emission tomography in prostate carcinoma" *Eur. J. Nucl. Med.,* **2000**, 27, 1415–1419

74. Kubota K, Yamada S, Ishiwata K, Ito M, Fujiwara T, Fukuda H, Tada M, Ido T, "Evaluation of the treatment response of lung cancer with positron emission tomography and L-[methyl-^{11}C]methionine: a preliminary study". *Eur J Nucl Med*. **1993**, 20(6), 495-501.

75. Bergstorm M, Bonasera TA, Lu L, Bergström E, Backlin C, Juhlin C, Långström B, "In Vitro and In Vivo Primate Evaluation of Carbon-11-Etomidate and Carbon-11-Metomidate as Potential Tracers for PET Imaging of the Adrenal Cortex and Its Tumors", *J. Nucl. Med*. **1998**, 39(6), 982-989

76. Chauveau F, Van Camp N, Dollé F, Kuhnast B, Hinnen F, Damont A, Boutin H, James M, Kassiou M, Tavitian B, "Comparative Evaluation of the Translocator Protein Radioligands ^{11}C-DPA-713, ^{18}F-DPA-714, and ^{11}C-PK11195 in a Rat Model of Acute Neuroinflammation", *J. Nucl. Med*., **2009**, 50(3), 468-476

77. Korkhov VM, Sachse C, Short JM, Tate CG, "Three-dimensional structure of TspO by electron cryomicroscopy of helical crystals." *Structure*, **2010**, 18(6), 677–687

78. Li F, Liu J, Zheng Y, Garavito MR, Ferguson-Miller S, "Crystal structures of translocator protein (TSPO) and mutant mimic of a human polymorphism." *Science,* **2015**, 347, 555–558

79. Lacapere JJ, Delavoie F, Li H, Péranzi G, Maccario J, Papadopoulos V, Vidic B, "Structural and functional study of reconstituted peripheral benzodiazepine receptor", *Biochem. Biophys. Res. Commun*., **2001**, 284(2), 536–541

80. Hardwick M, Fertikh D, Culty M, Li H, Vidic B, Papadopoulos V, "Peripheral-type benzodiazepine receptor (PBR) in human breast cancer: correlation of breast cancer cell aggressive phenotype with PBR expression, nuclear localization, and PBR-mediated cell proliferation and nuclear transport of cholesterol." *Cancer Res.,* **1999**, 59(4), 831-842.

81. Braestrup C, Squires RF, "Specific benzodiazepine receptors in rat brain characterized by high-affinity (3H) diazepam binding." *Proc. Natl. Acad. Sci. U.S.A*. **1977**, 74(9), 3805–3809

82. De Souza EB, Anholt RRH, Murphy KMM, Snyder SH, Kuhar MJ, "Peripheral-Type Benzodiazepine Receptors in Endocrine Organs: Autoradiographic Localization in Rat Pituitary, Adrenal, and Testis." *Endocrinology,* **1985**, *116*, 567–573

83. Zeineh N, Nagler R, Gabay M, Weizman A, Gavish M, "Effects of Cigarette Smoke on TSPO-related Mitochondrial Processes." *Cells*. **2019**, 8(7), 694.

84. Loth MK, Choi J, McGlothan JL, Pletnikov MV, Pomper MG, Guilarte TR, "TSPO in a murine model of Sandhoff disease: presymptomatic marker of neurodegeneration and disease pathophysiology." *Neurobiol Dis*. **2016**, 85, 174-186.

85. Gruber-Schoffnegger D, Drdla-Schutting R, Hönigsperger C, Wunderbaldinger G, Gassner M, Sandkühler J, "Induction of thermal hyperalgesia and synaptic long-term potentiation in the spinal cord lamina I by TNF-α and IL-1β is mediated by glial cells." *J Neurosci*. **2013**, 33(15), 6540-6551.

86. Chiu IM, von Hehn CA, Woolf CJ. "Neurogenic inflammation and the peripheral nervous system in host defense and immunopathology." *Nat Neurosci*., **2012**, 15(8), 1063-1067.

87. Beggs S, Liu XJ, Kwan C, Salter MW. Peripheral nerve injury and TRPV1-expressing primary afferent C-fibers cause opening of the blood-brain barrier. *Mol Pain*. **2010**;6, p. 74.

88. Tohidpour A, Morgun AV, Boitsova EB, Malinovskaya NA, Martynova GP, Khilazheva ED, Kopylevich NV, Gertsog GE, Salmina AB, "Neuroinflammation and Infection: Molecular Mechanisms Associated with Dysfunction of Neurovascular Unit." *Front Cell. Infect. Microbiol*. **2017**, 7, 276.

89. Kreutzberg GW. "Microglia: a sensor for pathological events in the CNS." Trends Neurosci. **1996**, 19(8), 312–318

90. Nimmerjahn A, Kirchhoff F, Helmchen F. "Resting microglial cells are highly dynamic surveillants of brain parenchyma in vivo." *Science,* **2005**, 308(5726), 1314–1318.

91. Graeber MB. "Glial inflammation in neurodegenerative diseases" *Immunology*, **2001**, 101(Suppl 1), 52

92. Ghadery C, Koshimori Y, Coakeley S, Harris M, Rusjan P, Kim J, Houle S, Strafella AP, "Microglial activation in Parkinson's disease using [^{18}F]-FEPPA." *J Neuroinflammation*. **2017**, 14(1), 8.

93. Cavedo E, Lista S, Khachaturian Z, Aisen P, Amouyel P, Herholz K, Jack CR, Sperling R, Cummings J, Blennow K, O'Bryant S, Frisoni GB, Khachaturian A, Kivipelto M, Klunk W, Broich K, Andrieu S, Thiebaut de Schotten M, Mangin J-F, Lammertsma AA, Johnson K, Teipel S, Drzezga A, Bokde A, Colliot O, Bakardjian H, Zetterberg H, Dubois B, Vellas B, Schneider LS, Hampel H, "The Road Ahead to Cure Alzheimer's Disease: Development of Biological Markers and Neuroimaging Methods for Prevention Trials Across all Stages and Target Populations." *J Prev Alzheimers Dis*. **2014**, 1(3), 181-202.

94. Marcus C, Mena E, Subramaniam RM. "Brain PET in the diagnosis of Alzheimer's disease." *Clin Nucl Med*. **2014**, 39(10), 413–426

95. Mosconi L. "Glucose metabolism in normal aging and Alzheimer's disease: Methodological and physiological considerations for PET studies." *Clin Transl Imaging*. **2013**, 1(4),

96. Klunk WE, Engler HA. Nordberg A, Wang Y, Blomqvist G, Holt DP, Bergström M, Savitcheva I, Huang G-F, Estrada S, Ausén B, Debnath ML, Barletta J, Price JC, Sandell J, Lopresti BJ, Wall A, Koivisto P, Antoni G, Mathis CA, Långström B, "Imaging brain amyloid in Alzheimer's disease with Pittsburgh compound-B." *Ann. Neurol.* **2004**, 55(3), 306–319.

97. Jaremko L, Jaremko M, Giller K, Becker S, Zweckstetter M, "Structure of the mitochondrial translocator protein in complex with a diagnostic ligand". *Science*, **2014**, 343(6177), 1363–1366

98. Petit-Taboué, M-C, Baron J-C, Barré L, Travère J-M, Speckel D, Camsonne R, MacKenzie ET, "Brain kinetics and specific binding of [^{11}C]PK 11195 to ω_3 sites in baboons: positron emission tomography study", *Eur. J. Pharmacol*., **1991**, 200(2-3), 347-351

99. Banati RB, Newcombe J, Gunn RN, Cagnin A, Turkheimer F, Heppner F, Price G, Wegner F, Giovannoni G, Miller DH, Perkin GD, Smith T, Hewson AK, Bydder G, Kreutzberg GW, Jones T, Cuzner ML, Myers R, "The peripheral benzodiazepine binding site in the brain in multiple sclerosis: Quantitative *in vivo* imaging of microglia as a measure of disease activity", *Brain*, **2000**, 123(11), 2321–2337

100. Owen DR, Yeo AJ, Gunn RN, Song K, Wadsworth G, Lewis A, Rhodes C, Pulford DJ, Bennacef I, Parker CA, StJean PJ, Cardon LR, Mooser VE, Matthews VM, Rabiner EA, Rubio JP, "An 18-kDa Translocator Protein (TSPO) Polymorphism Explains Differences in Binding Affinity of the PET Radioligand PBR28", *J. Cereb. Blood. Flow. Metab.,* **2011**, 32(1), 1-5

101. Parente A, Kopschina Feltes P, Vállez García D, Sijbesma JWA, CM Moriguchi Jeckel, Dierckx RAJO, de Vries EFJ, Doorduin J, "Pharmacokinetic analysis of ^{11}C-PBR28 in the rat model of herpes encephalitis: comparison with (R)-^{11}C-PK11195", *J.*

Nucl. Med., **2016**, 57(5), 785-791.

102. Boutin H, Chauveau F, Thominiaux C, Grégoire M-C, James ML, Trebossen R, Hantraye P, Dollé F, Tavitian B, Kassiou M, "^{11}C-DPA-713: A Novel Peripheral Benzodiazepine Receptor PET Ligand for In Vivo Imaging of Neuroinflammation"*, J. Nucl. Med.,* **2007**, 48(4), 573-581

103. Fookes CJR, Pham TQ, Mattner F, Greguric I, Loc'h C, Liu X, Berghofer P, Shepherd R, Gregoire M-C, Katsifis A, "Synthesis and biological evaluation of substituted [^{18}F]imidazo[1,2-a]pyridines and [^{18}F]pyrazolo[1,5-a]pyrimidines for the study of the peripheral benzodiazepine receptor using positron emission tomography." *J Med Chem*. **2008**, 51(13), 3700-3712

104. Boutin H, Prenant C, Maroy R, Galea J, Greenhalgh AD, Smigova A, Cawthorne C, Julyan P, Wilkinson SM, Banister SD, Brown G, Herholz K, Kassiou M, Rothwell NJ, "[^{18}F]DPA-714: direct comparison with [^{11}C]PK11195 in a model of cerebral ischemia in rats". *PLoS One*. **2013**, 8(2), 56441

105. Doorduin J, Klein HC, Dierckx RA, James M, Kassiou M, de Vries EF, "[^{11}C]-DPA-713 and [^{18}F]-DPA-714 as new PET tracers for TSPO: a comparison with [^{11}C]-(R)-PK11195 in a rat model of herpes encephalitis." *Mol Imaging Biol.* **2009**, 11(6), 386–398

106. Selleri S, Bruni F, Costagli C, Costanzo A, Guerrini G, Ciciani G, Costa B, Martini C, "2-Arylpyrazolo [1,5-a] pyrimidin-3-yl Acetamides. New Potent and Selective Peripheral Benzodiazepine Receptor Ligands." *Bioorg Med Chem*. **2001**, 9(10), 2661–2671.

107. Damont A, Médran-Navarrete V, Cacheux F, Kuhnast B, Pottier G, Bernards N, Marguet F, Puech F, Boisgard R, Dollé F, "Novel Pyrazolo[1,5-a]pyrimidines as Translocator Protein 18 kDa (TSPO) Ligands: synthesis, in vitro biological evaluation, [^{18}F]-labeling, and in vivo neuroinflammation PET Images." *J Med Chem*. **2015**, 58(18), 7449–7464.